



**The Abdus Salam
International Centre for Theoretical Physics**



2240-18

**Advanced School on Scaling Laws in Geophysics: Mechanical and
Thermal Processes in Geodynamics**

23 May - 3 June, 2011

Topography and Dynamic Topography

Shijie ZHONG

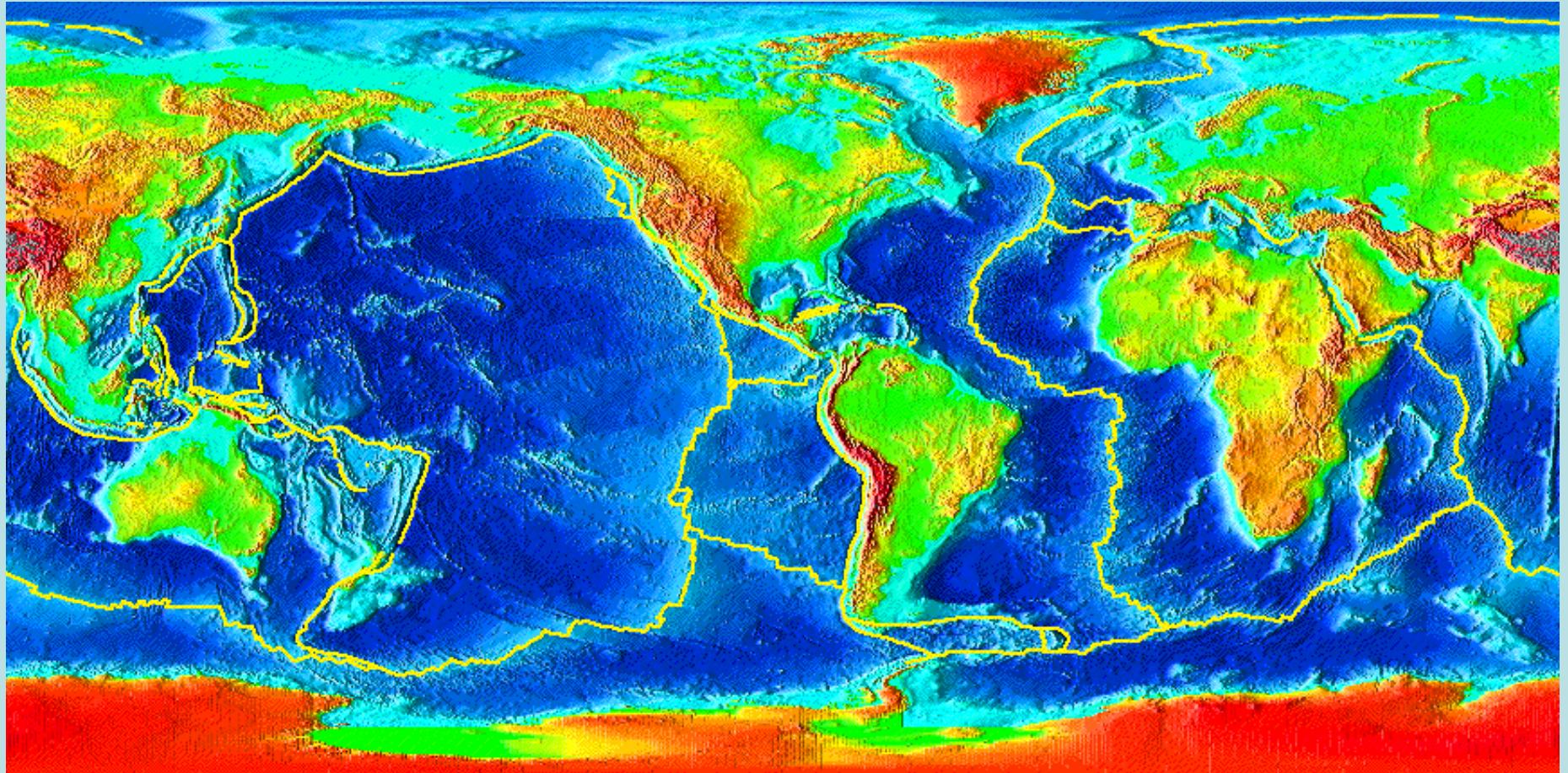
*Department of Physics
University of Colorado, Boulder
Colorado
U.S.A.*

Topography and Dynamic Topography

Shijie Zhong

**Department of Physics
University of Colorado
Boulder, Colorado
USA**

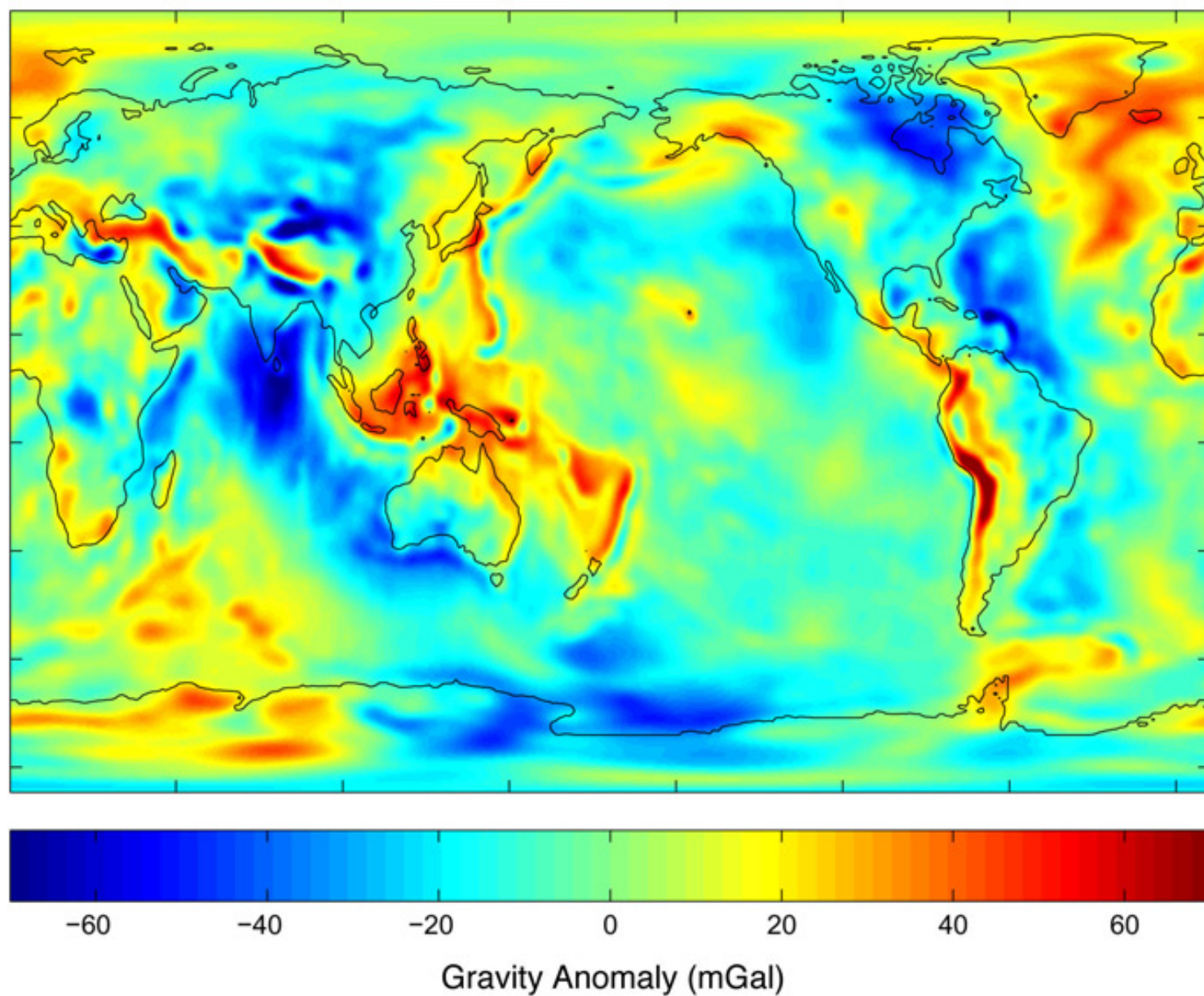
**ICTP Advanced School on Scaling Laws in Geophysics
5/31 and 6/1, 2011**



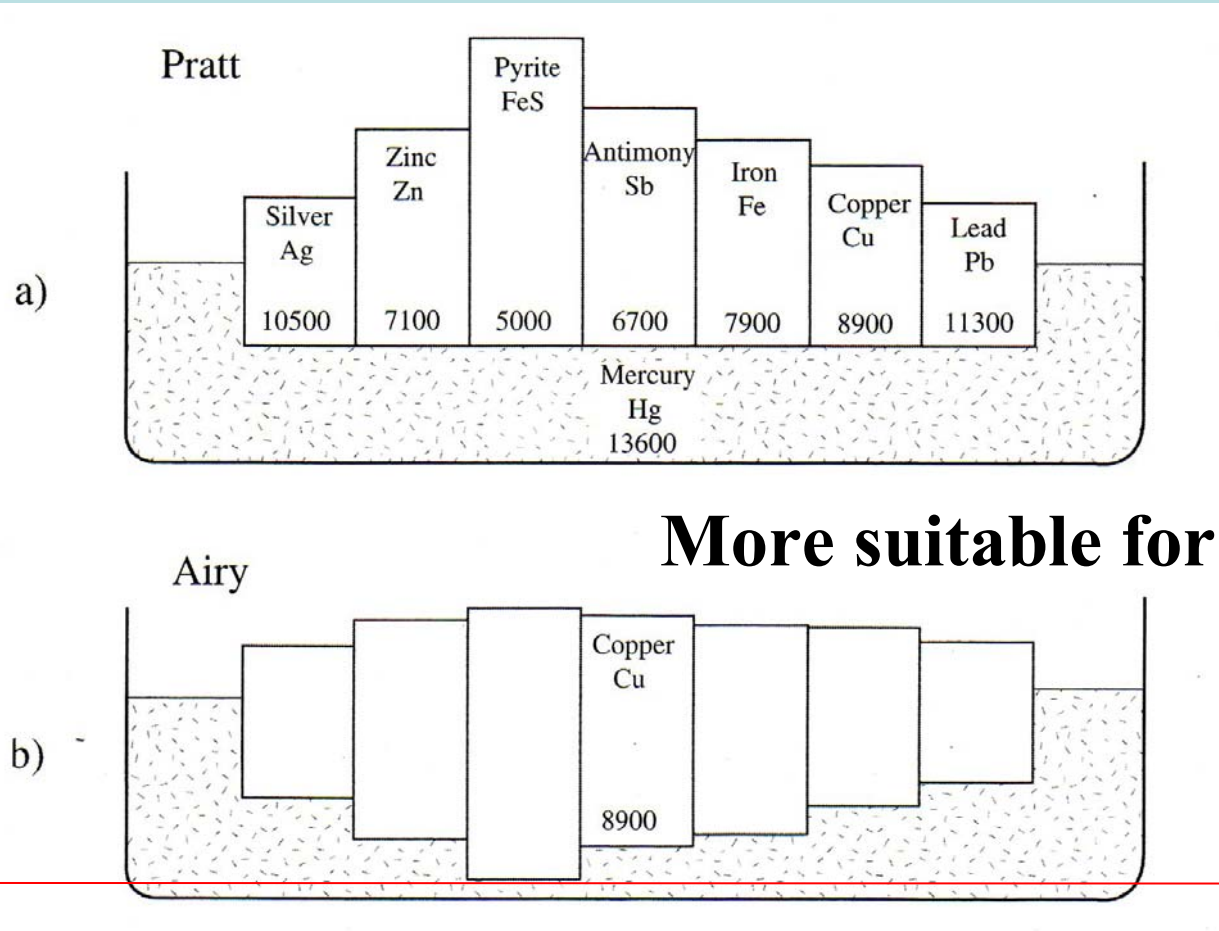
Origins for the topography

- 1) Crust and lithosphere (isostatic).**
- 2) Sub-lithosphere (non-isostatic or dynamic).**

Free-air gravity anomalies



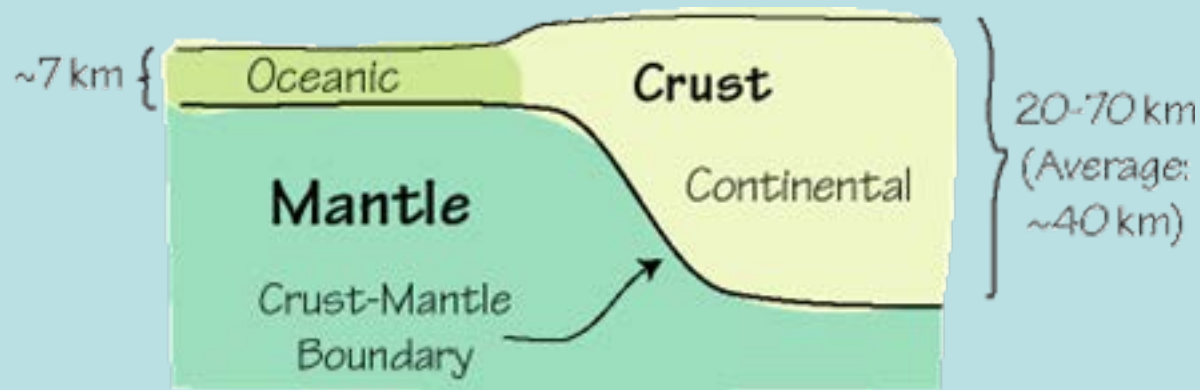
Pratt and Airy Models of Isostasy



More suitable for continents

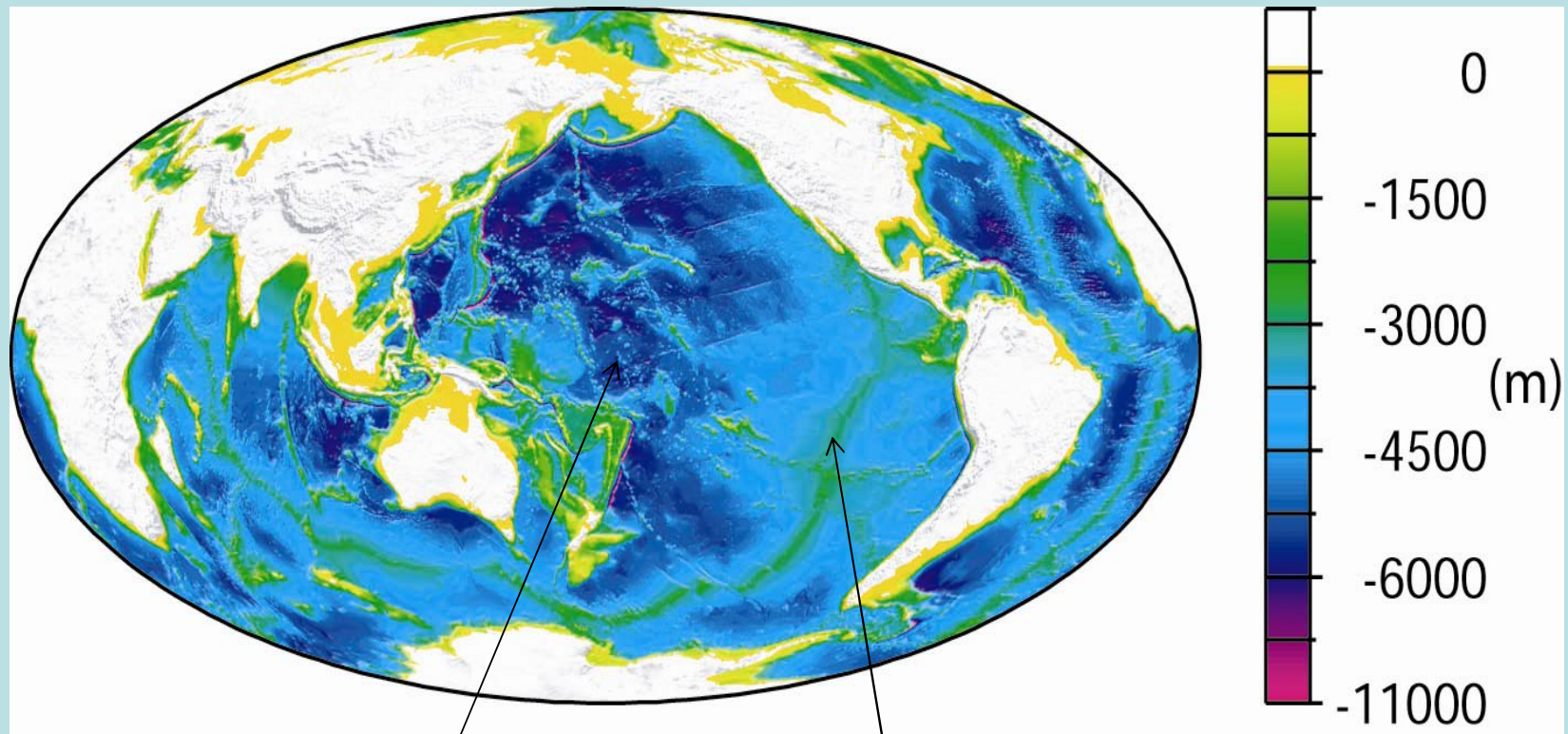
**Compensation depth
with equal pressure**

Topography due to crustal thickness variations



For a perfect Airy isostasy, for 1 km surface topography high, the Moho is expected to be depressed by $\rho_{\text{cont}}/(\rho_{\text{m}}-\rho_{\text{cont}}) \sim 5.6$ km.

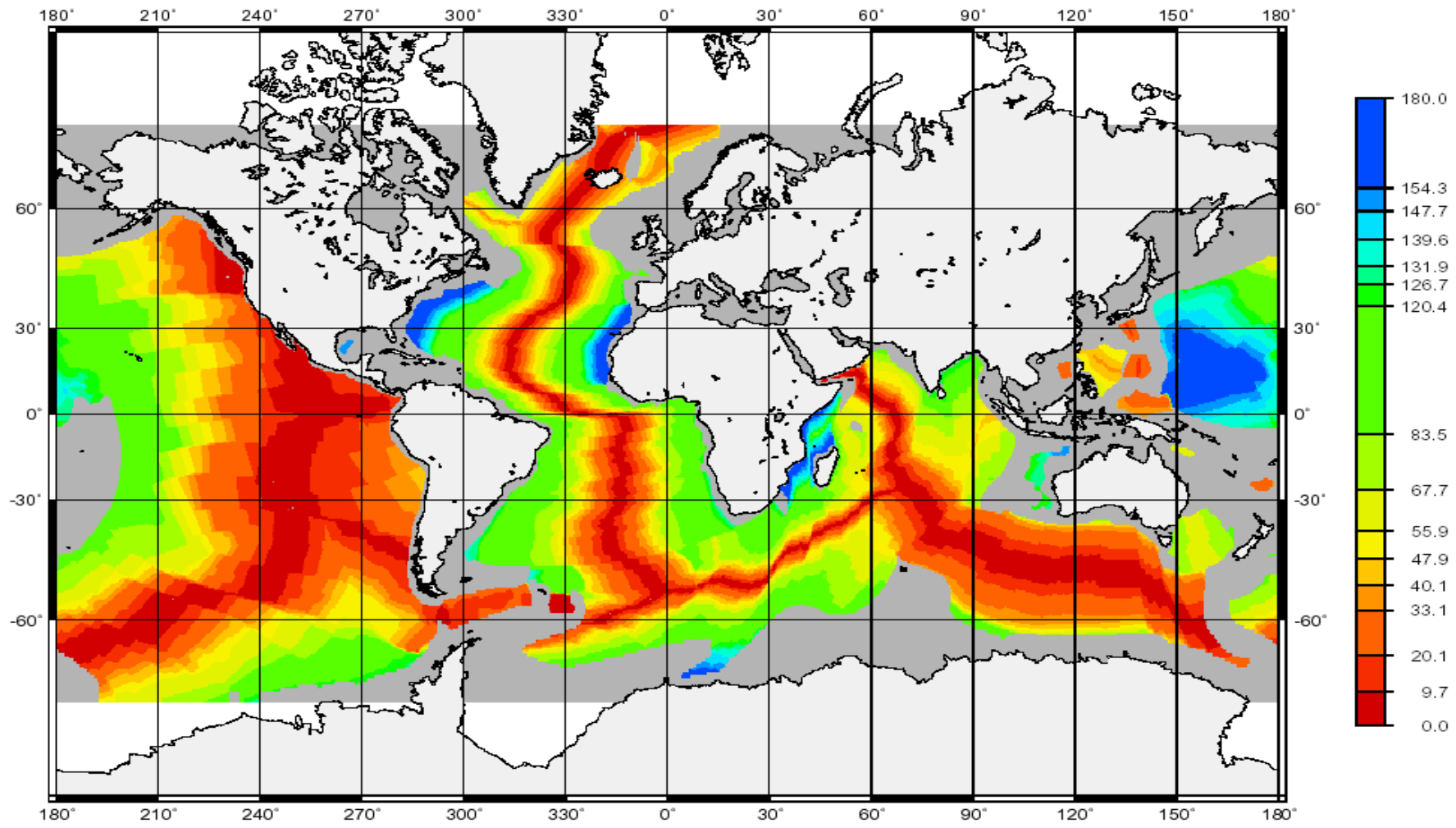
Topography variations on seafloor



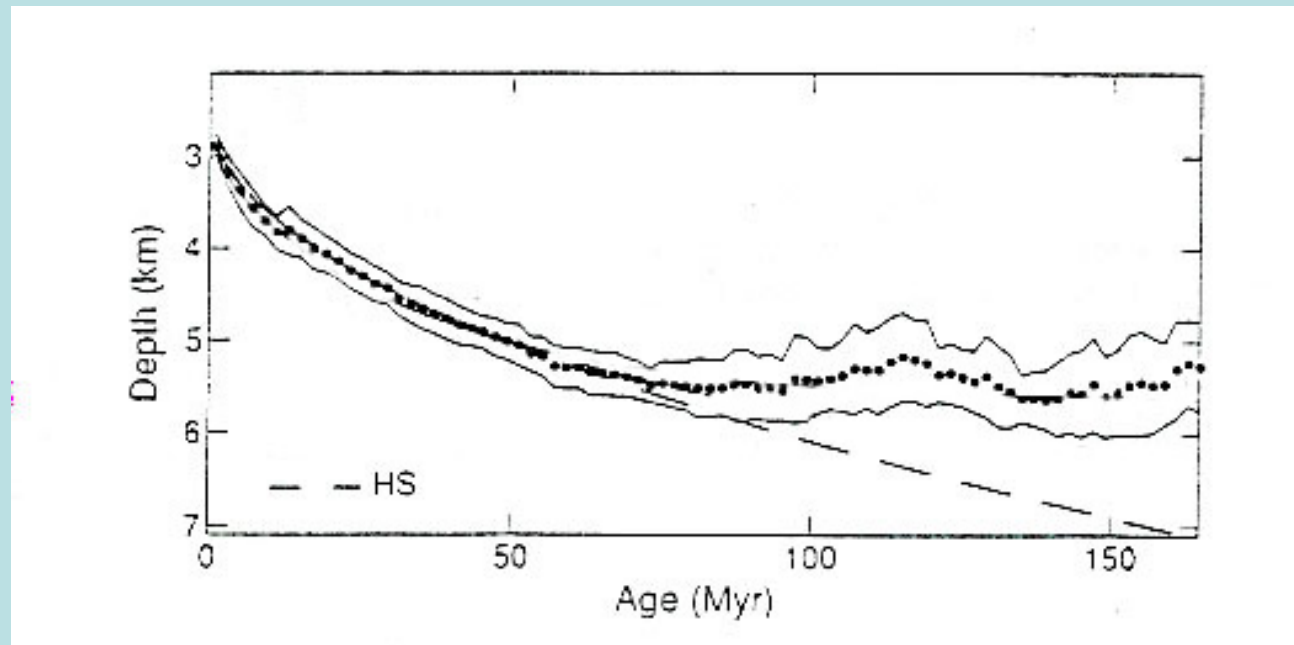
ocean basins

Mid-ocean ridges

Age of Ocean floor



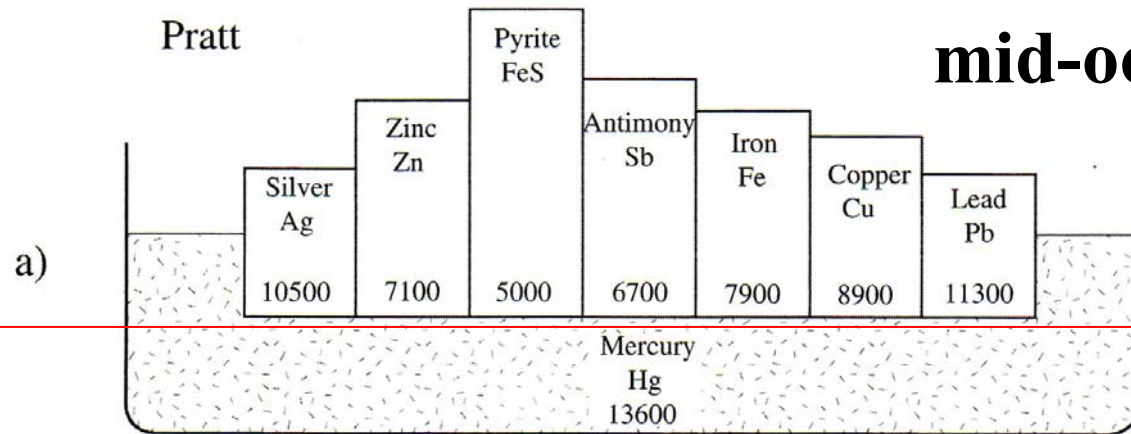
Age-dependent Ocean Depth (Parsons & Sclater, 1977)



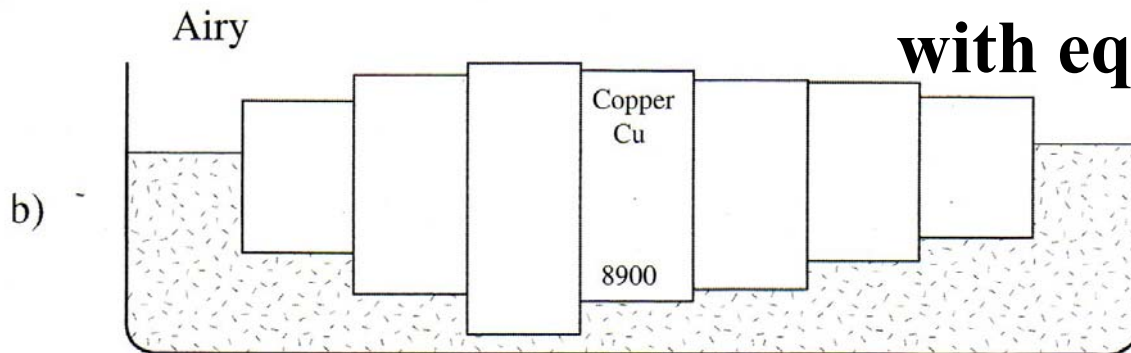
Stein and Stein, 1992

Pratt and Airy Models of Isostasy

More suitable for mid-ocean ridges

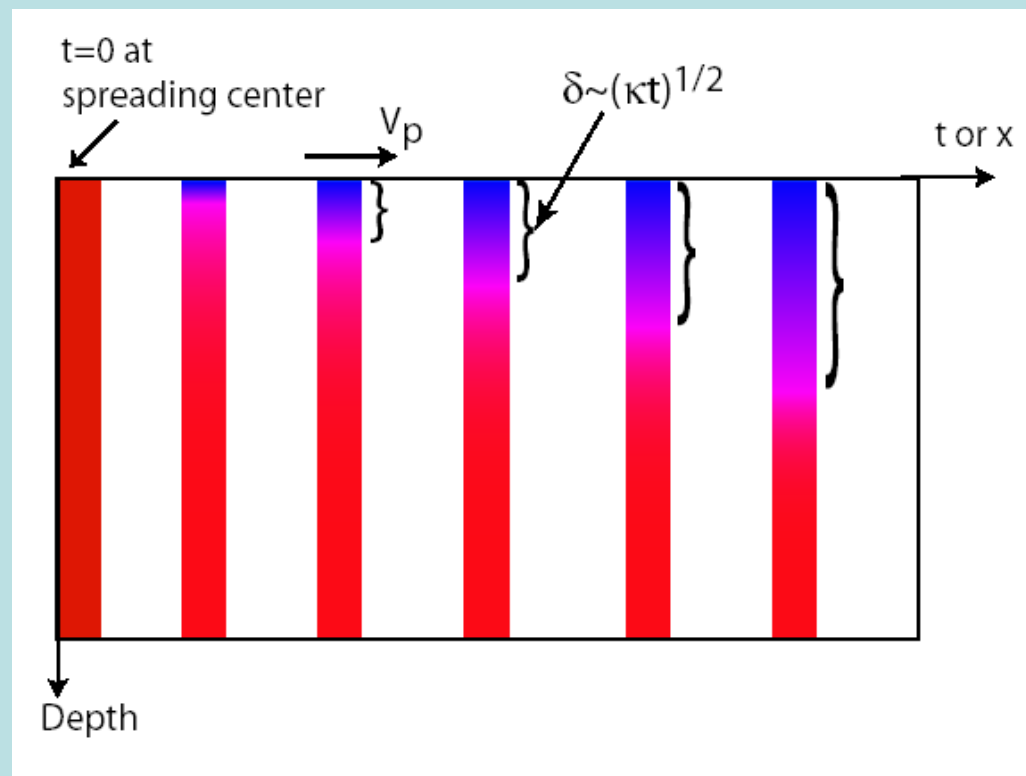


Compensation depth with equal pressure



A Simple Model for Age-dependent Topography and Heat Flux (a half-space cooling model)

- Conductive cooling of oceanic lithosphere as it moves away from the spreading centers [Turcotte & Oxburgh, 1967].



Temperature:

$$T = T_s + (T_m - T_s) \operatorname{erf}[y / (4\kappa t)^{1/2}]$$

Heat flux:

$$Q_s \sim (T_m - T_s) / \delta$$

$$\text{or } Q_s = k(T_m - T_s) / (\kappa t)^{1/2}$$

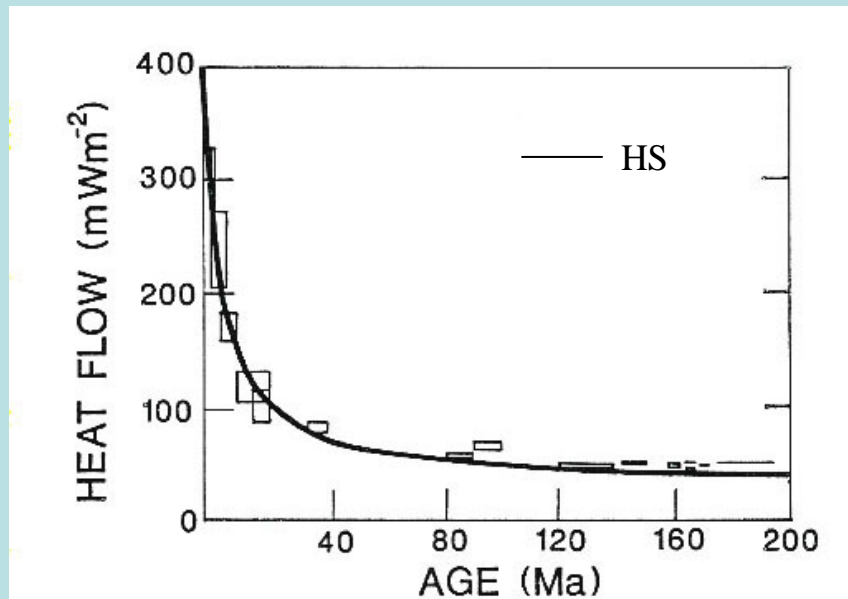
Topography:

$$w = 2b\alpha(T_m - T_s)(\kappa t / \pi)^{1/2}$$

$$\text{where } b = \rho_m / (\rho_m - \rho_w)$$

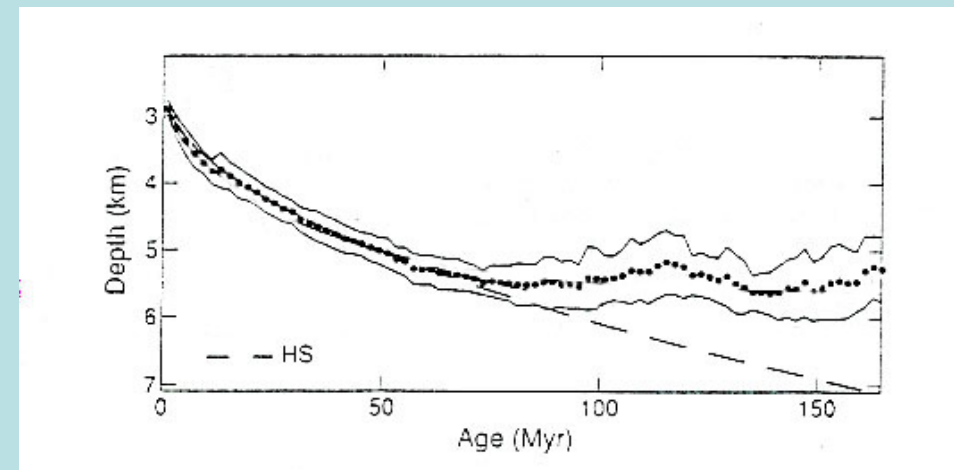
Fit to Ocean Depth and Heat Flux from $\frac{1}{2}$ Space Cooling Model

Heat Flux



Lister et al., 1991

Ocean Depth

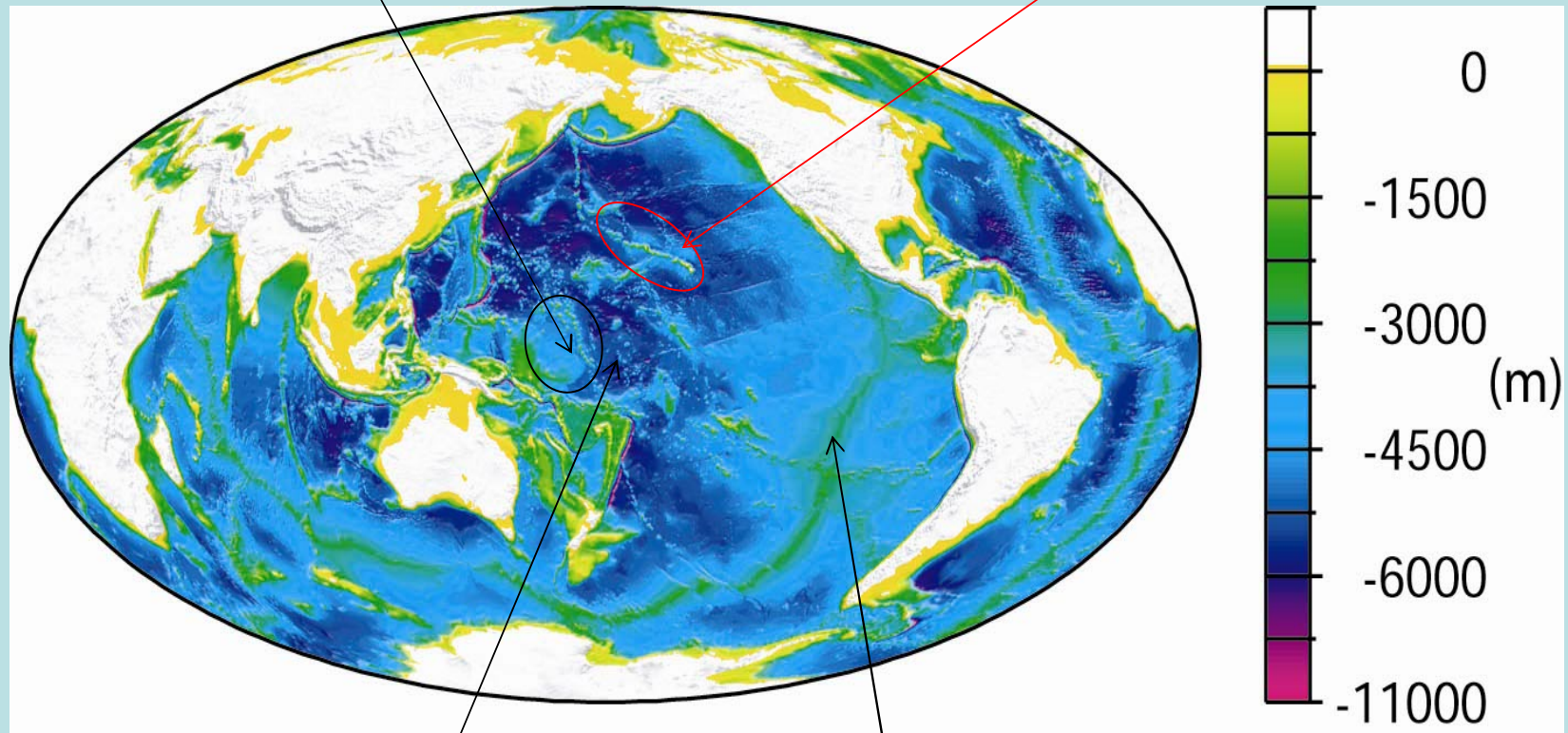


Stein and Stein, 1992

Topography variations on seafloor

Ontong Java plateau

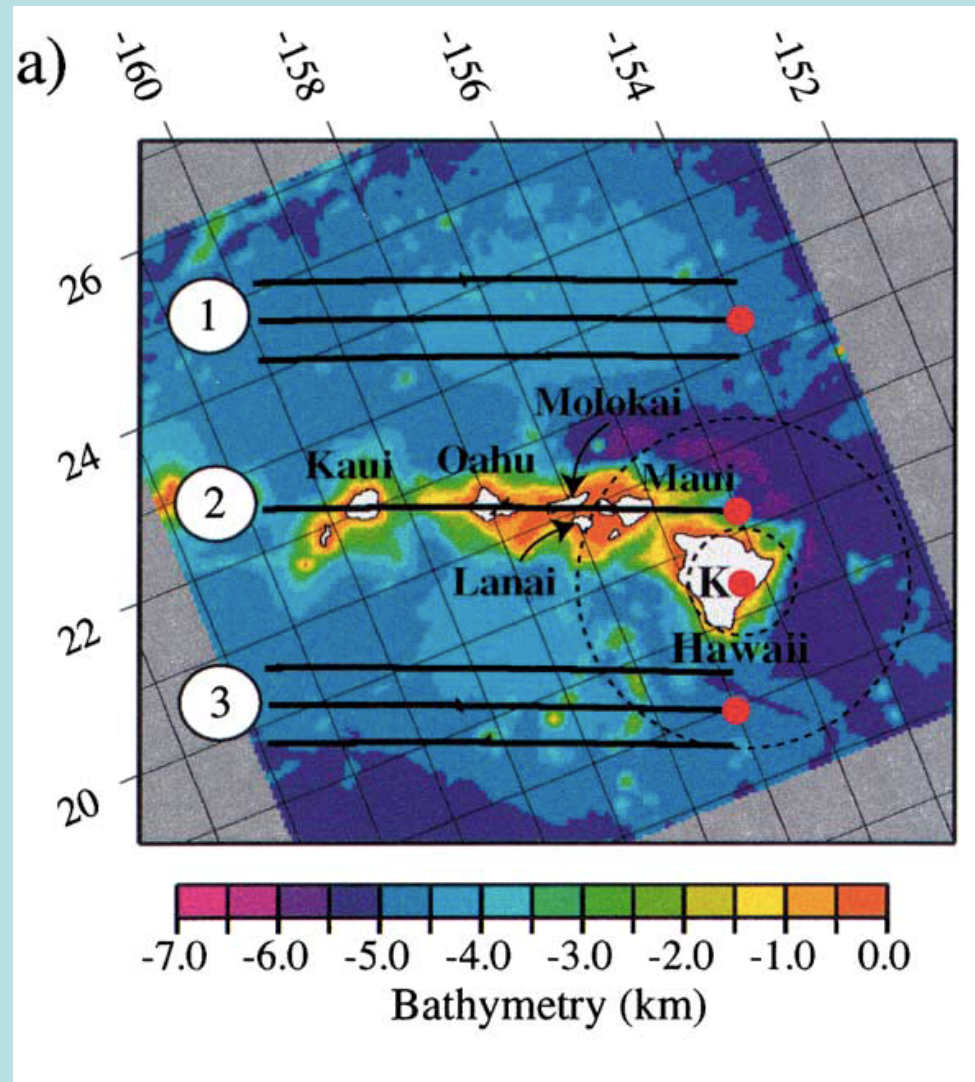
Hawaiian swell



ocean basins

Mid-ocean ridges

Hawaiian swell topography from sub-lithospheric sources



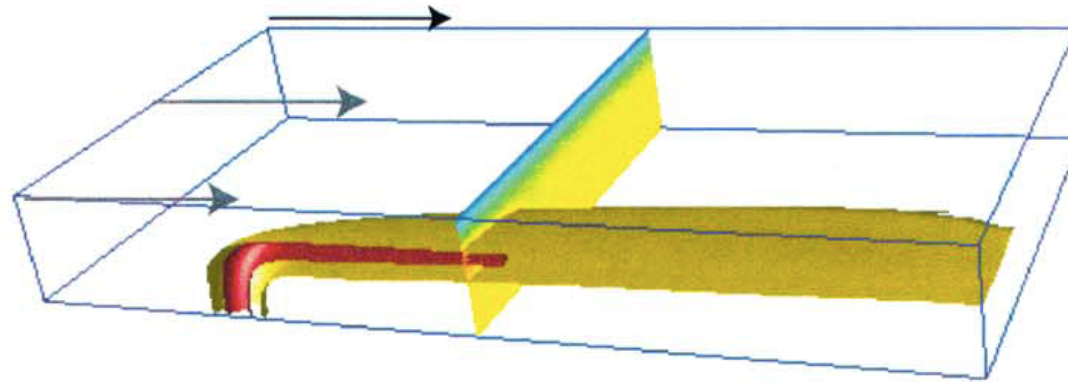
**~1 km high,
>1000 km wide.**

**Normal crustal
thickness.**

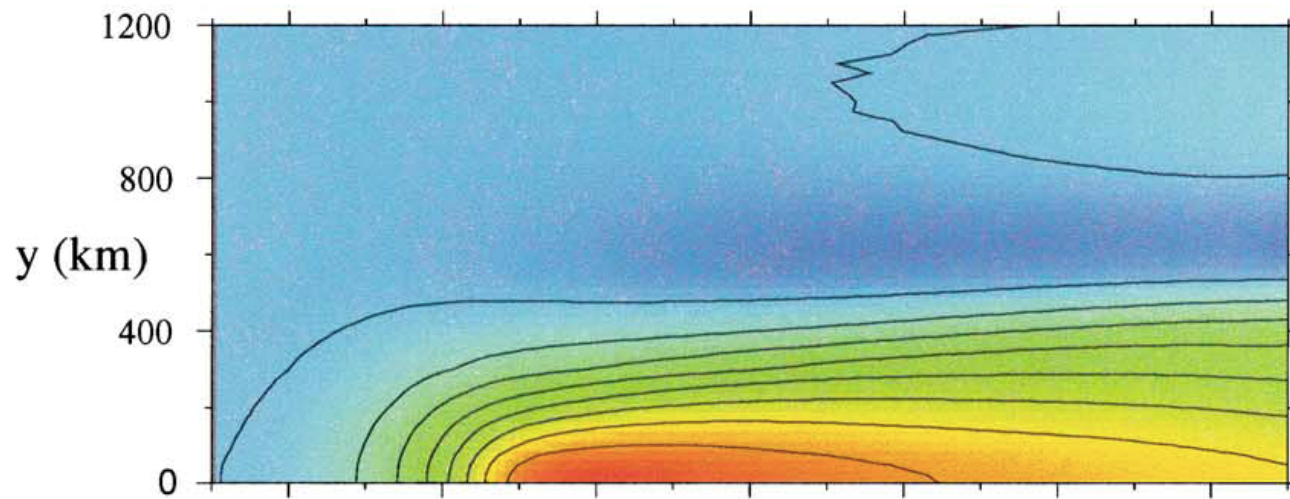
A mantle plume for the Hawaiian swell

(Ribe & Christensen, 1994; Zhong & Watts, 2002)

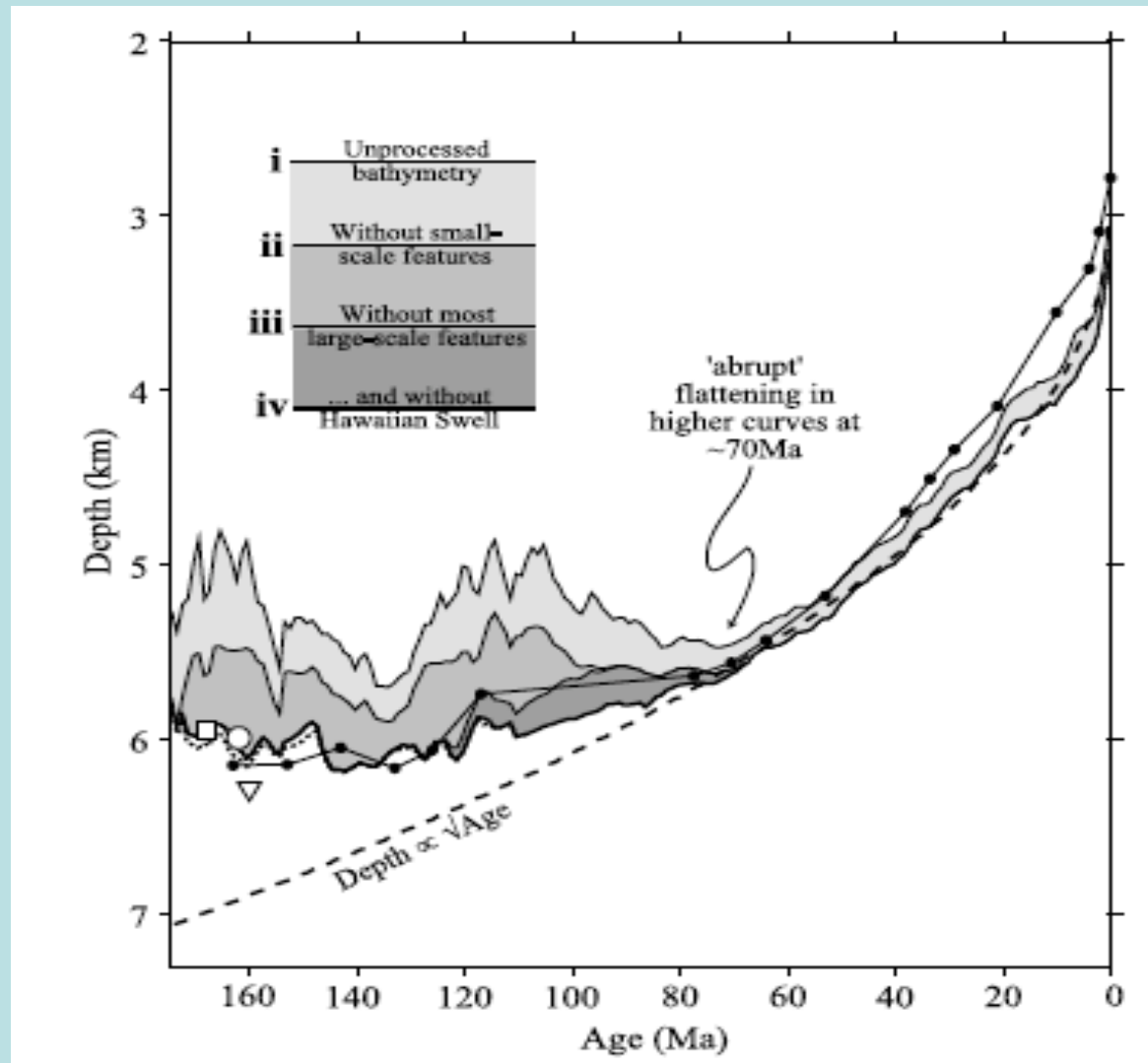
a) Thermal structure



b) Swell planform



Corrected for surface features (e.g., seamounts, ...)

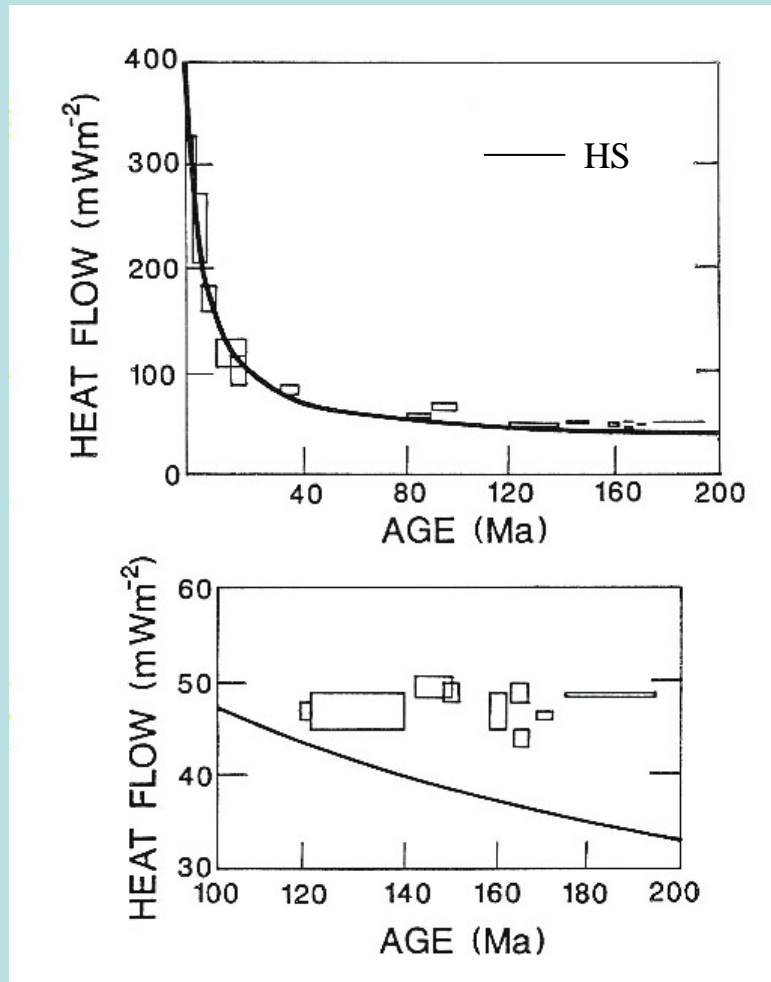


Northern Pacific

Hillier & Watts, 2005

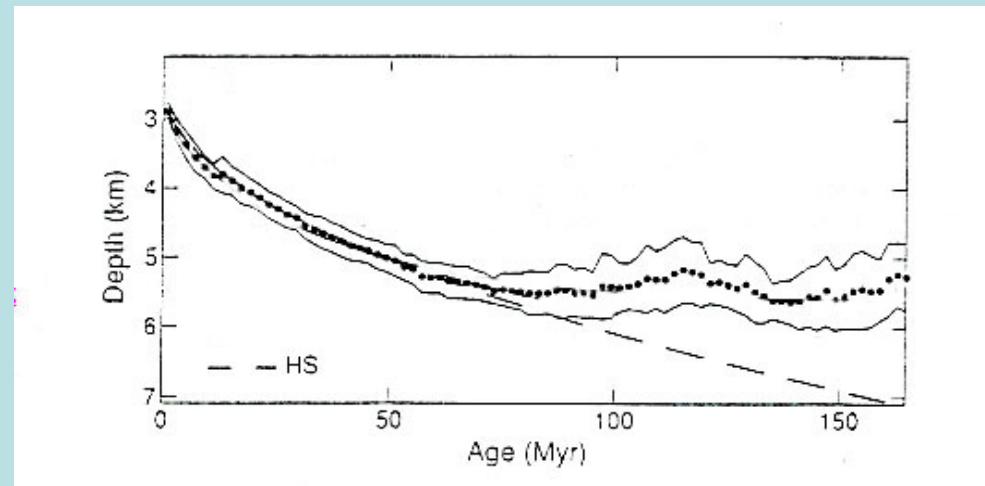
The half-space cooling model: The fit to and deviations from the observations

Heat Flux



Lister et al., 1991

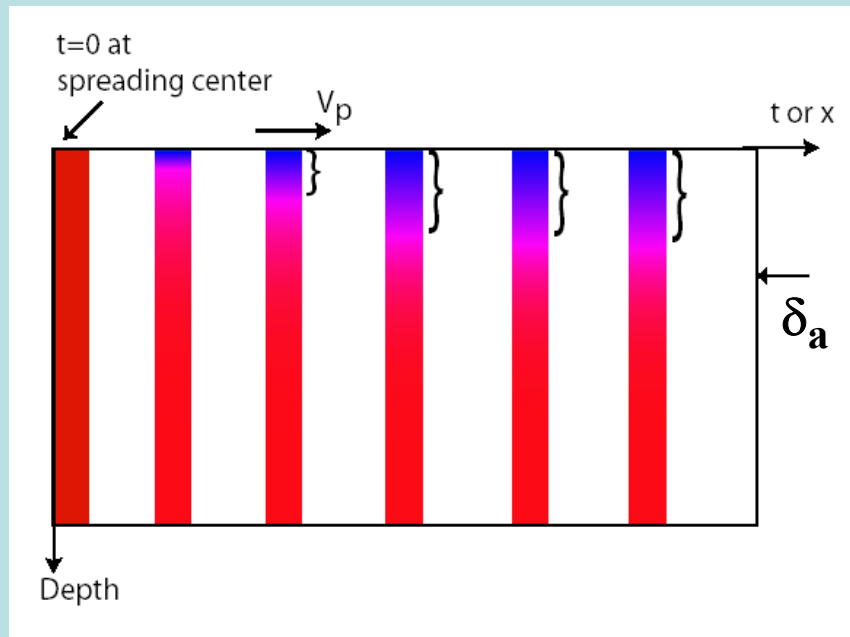
Ocean Depth



Stein and Stein, 1992

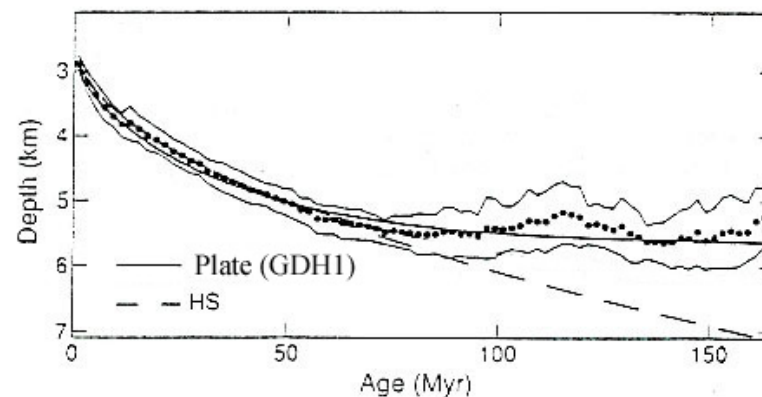
The Plate Model – a revised model to fit the data

[Parsons & Sclater, 1977; Parsons & McKenzie, 1978]

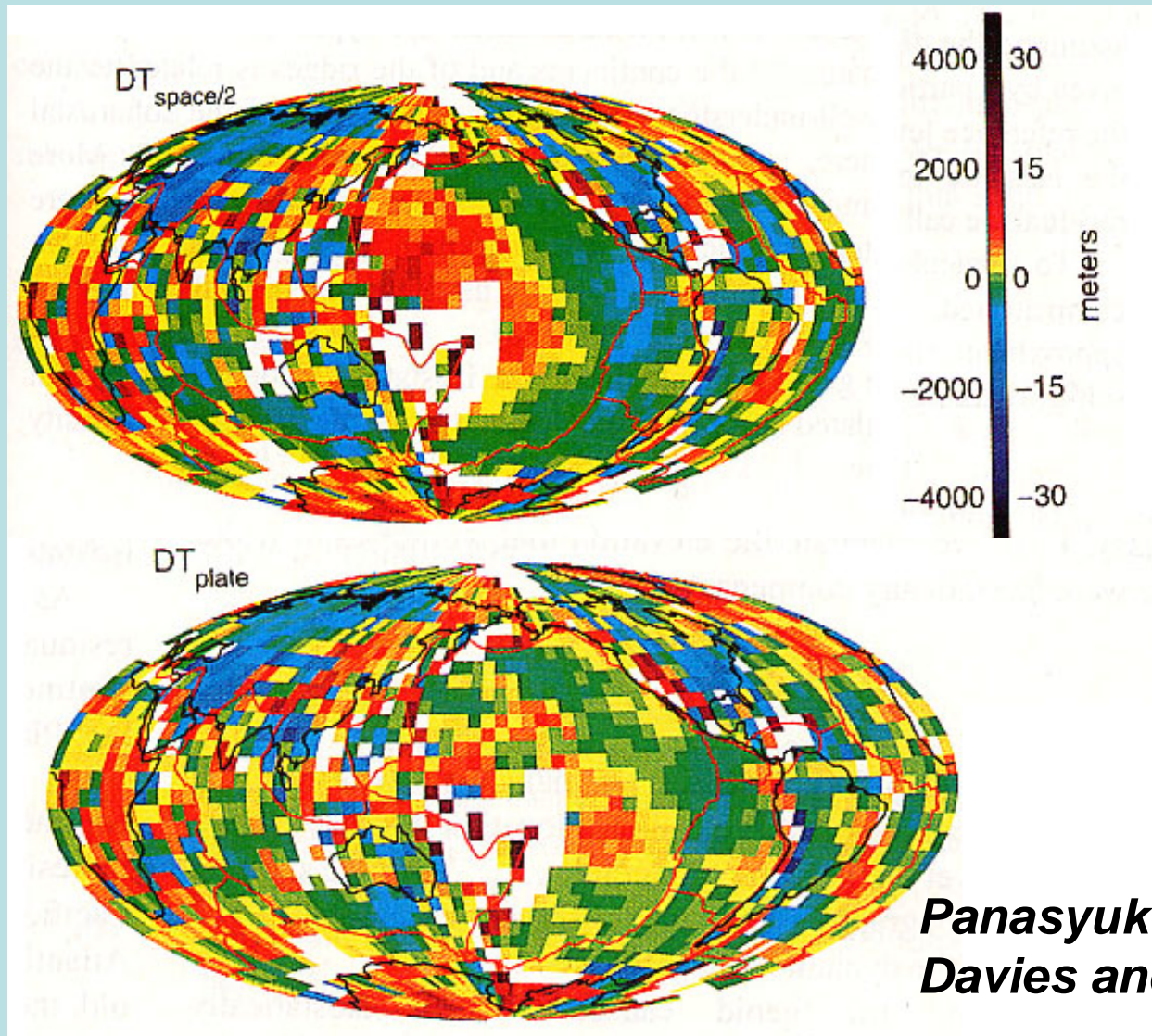


Assuming that there is an upper limit on δ , δ_a . And the cooling never reaches to depth of δ_a .

Stein & Stein, 1992

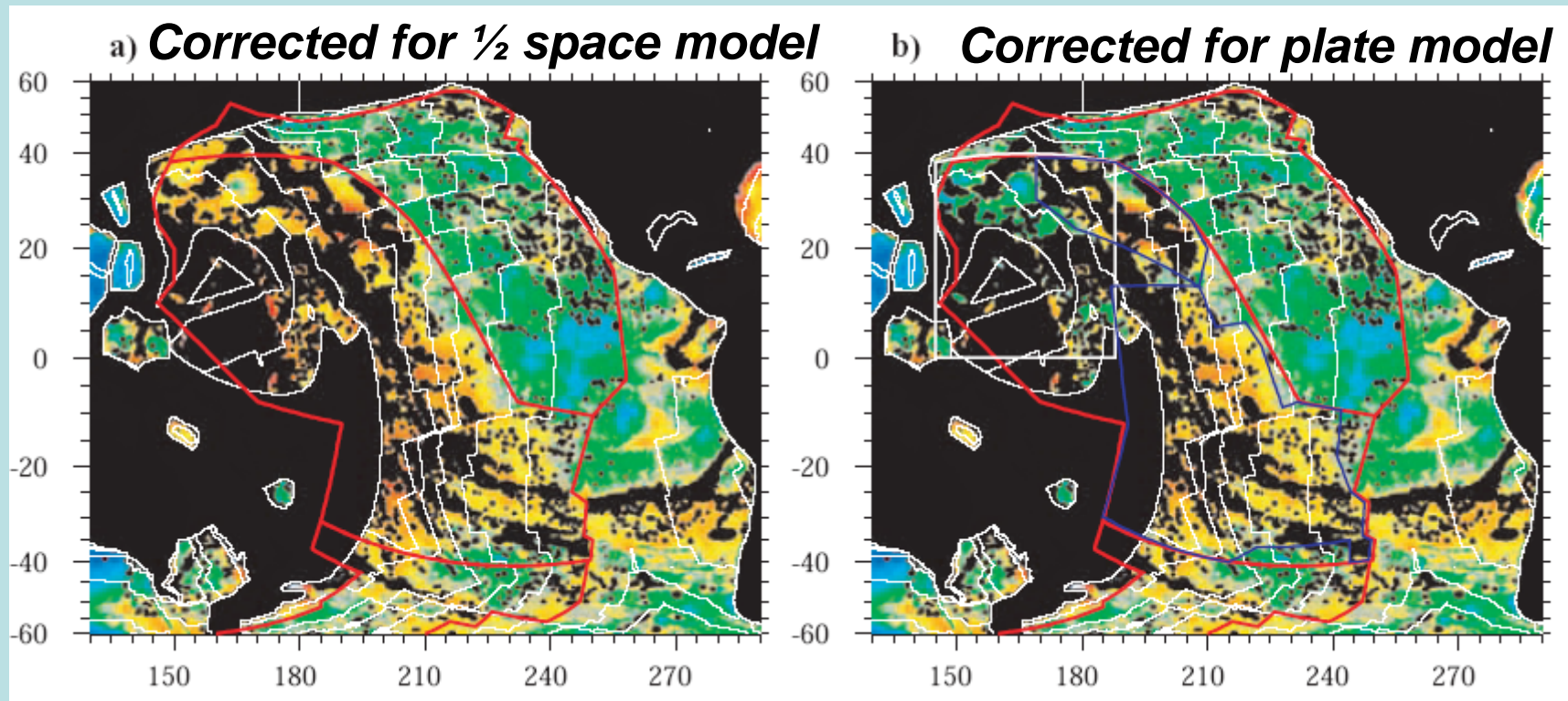


Age is not the only control!
Residual/dynamic topography (Pacific and African
superswells)



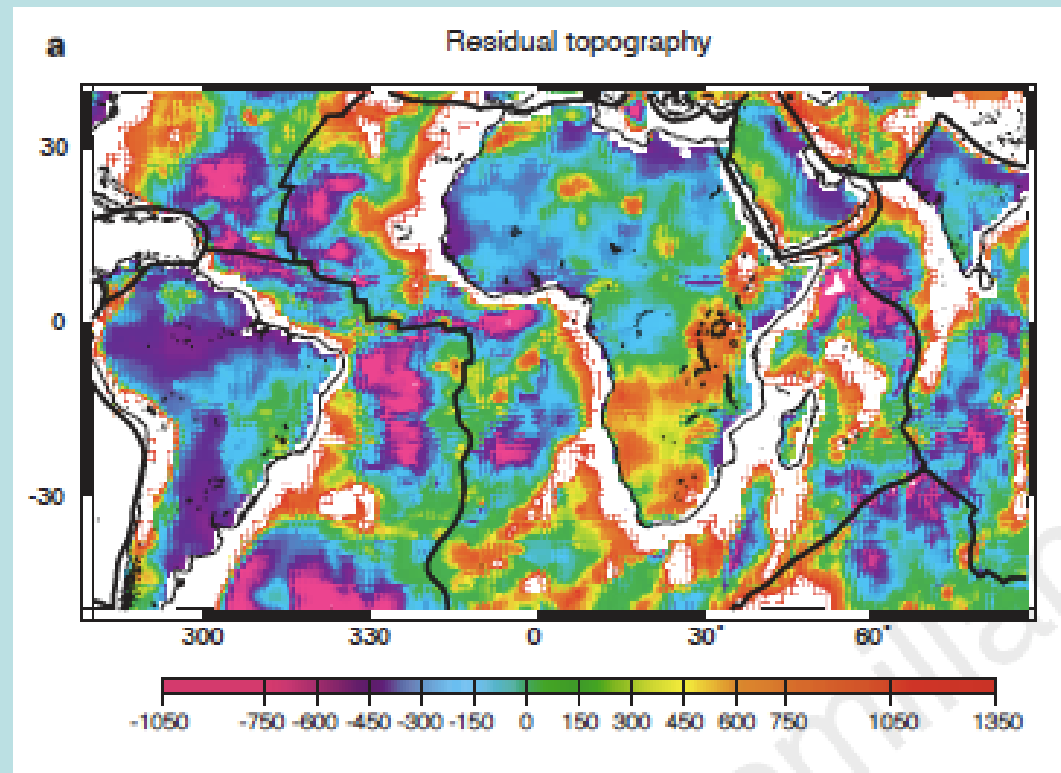
*Panasyuk & Hager, 2000;
Davies and Pribac, 1993*

Age is not the only control!
-- Residual/dynamic topography



Zhong et al., 2007

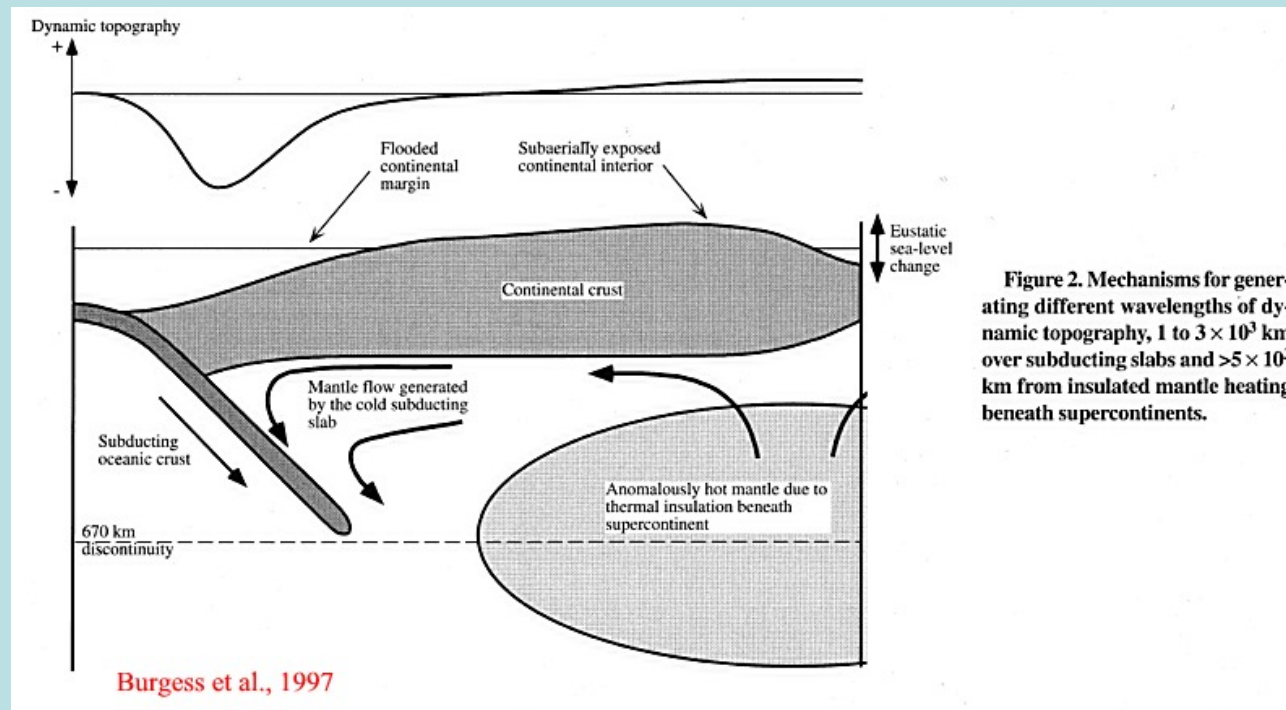
African swell – residual topography relative to $\frac{1}{2}$ space cooling model



***Nybrade & Robinson, 1994;
Lithgow-Bertelloni & Silver, 1998***

Dynamic topography

- Topography generated by the dynamics of mantle flow.



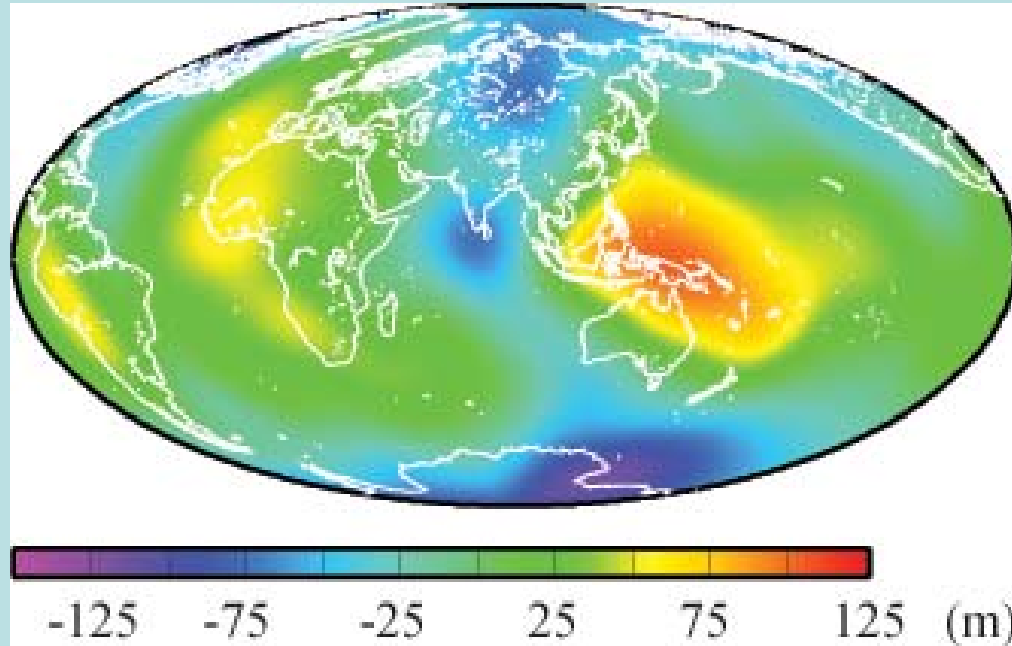
Origins for the topography

- 1) **Crust and lithosphere (isostatic).**
- 2) **Sub-lithosphere (non-isostatic or dynamic).**

***Dynamic topography* is that due to non-isostatic (i.e., non-crustal and non-lithospheric) effects, i.e., *residual topography* after correcting for isostatic effects or crustal and lithospheric contributions to the topography.**

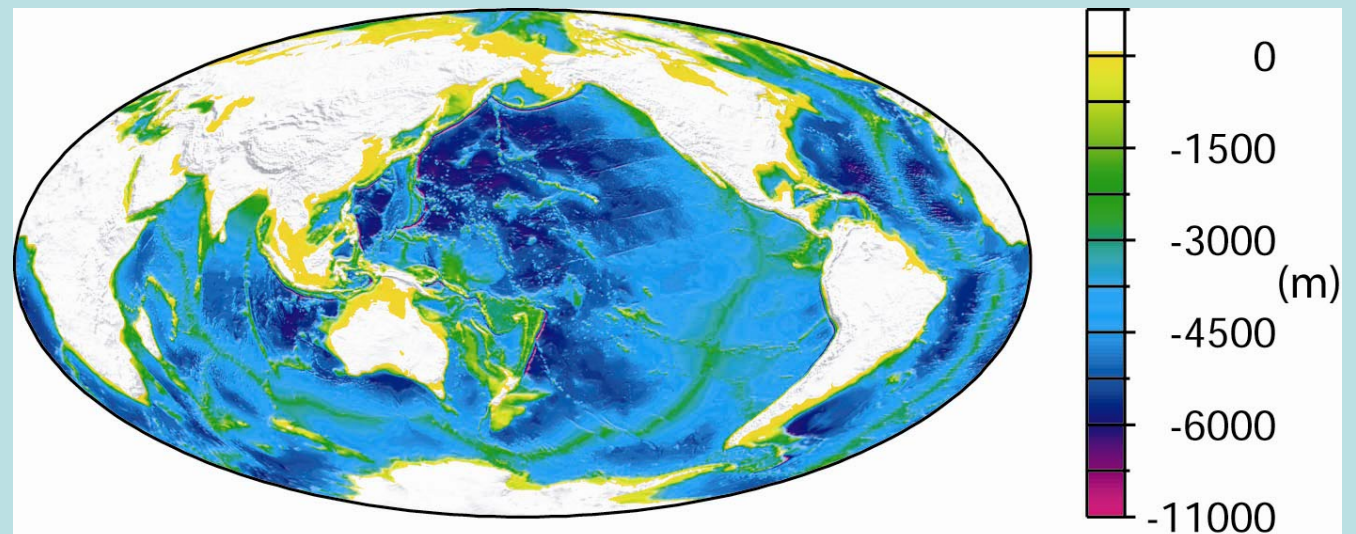
***Dynamic topography* is important because it tells us about the dynamics. It is also more difficult to get because some tricky “corrections” are needed.**

Make a case for dynamic topography for the Pacific and African superswells



Generally reflect distribution of mass anomalies.

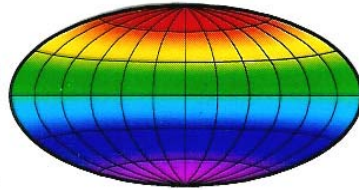
No clear correlation with ocean-continent contrast.



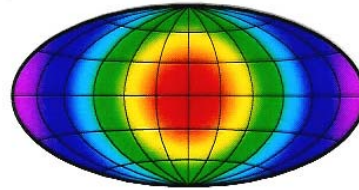
Spherical harmonic functions $Y_{lm}(\theta, \phi)$

Degree 1:

Y_{10}

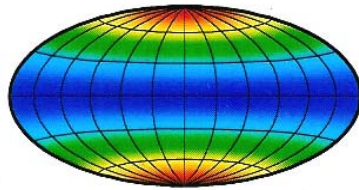


Y_{11}

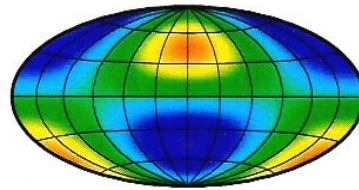


Degree 2:

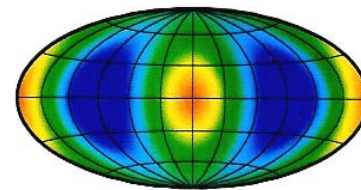
Y_{20}



Y_{21}



Y_{22}



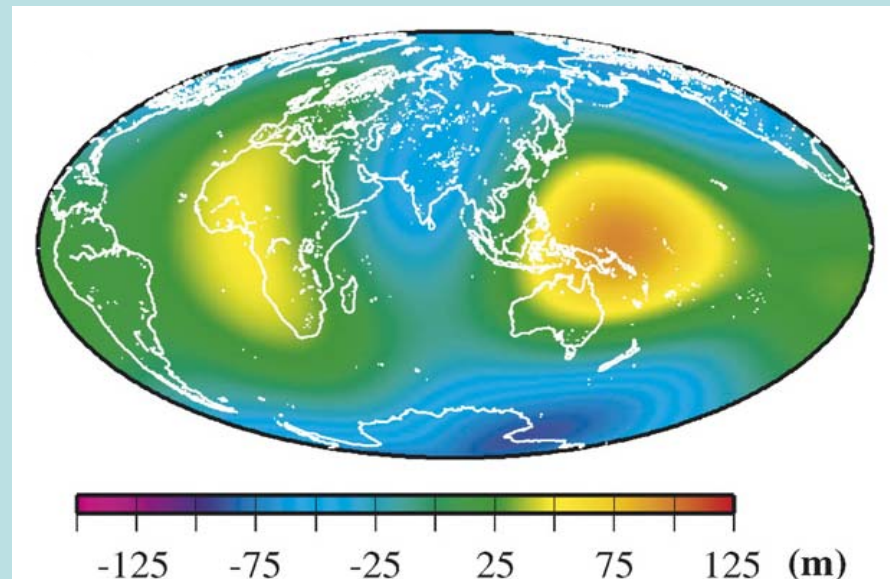
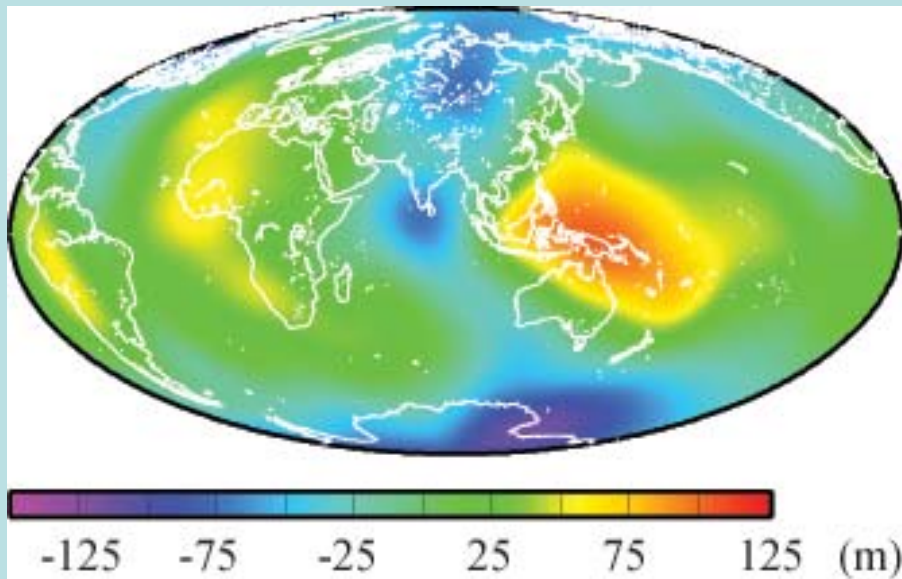
Degree 3:

Wavelength $\sim 40000/l$ (km)

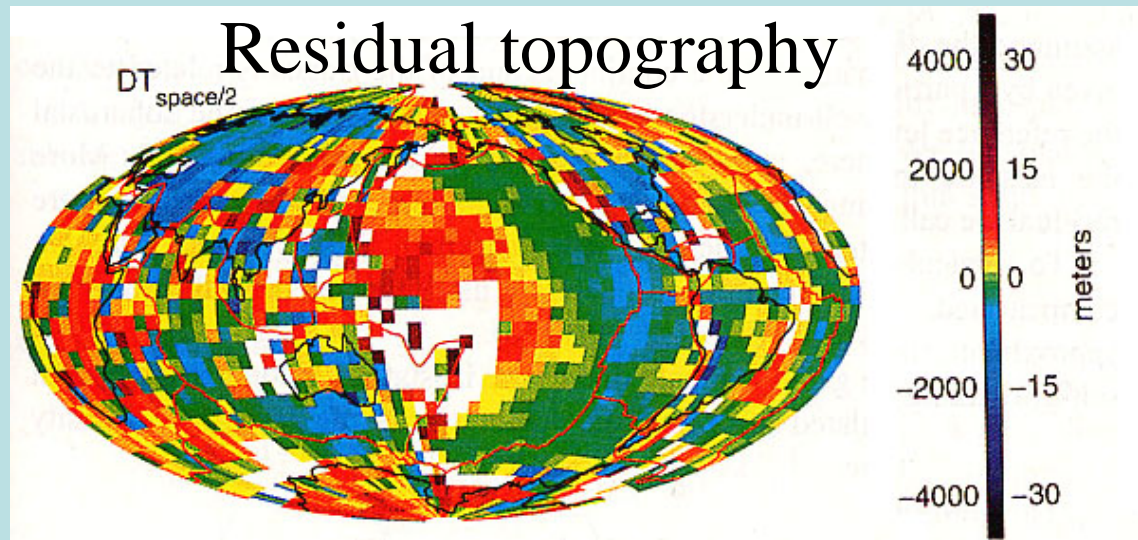
The Earth's geoid (gravity) anomalies

$$N(\theta, \phi) = \frac{GM}{Rg} \left\{ \sum_{l=2}^L \sum_{m=0}^l [C_{lm} \cos(m\phi) + S_{lm} \sin(m\phi)] P_{lm}(\cos \theta) \right\}$$

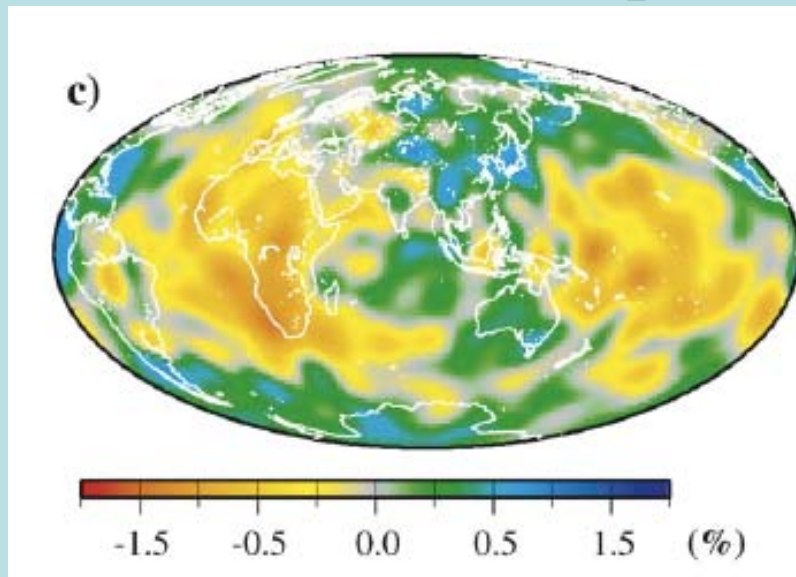
Long-wavelength geoid (degrees $l=2$ and 3)



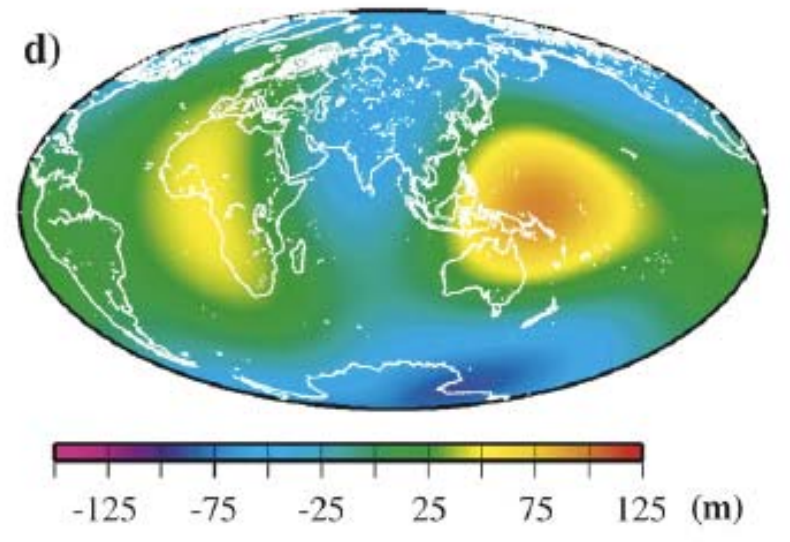
A case for dynamic topography



dV_s/V_s at 2300 km depth

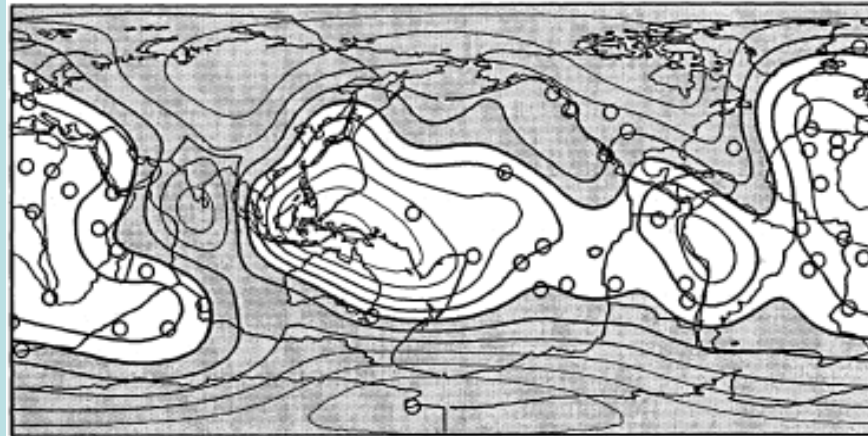


Geoid anomalies (1=2 & 3)

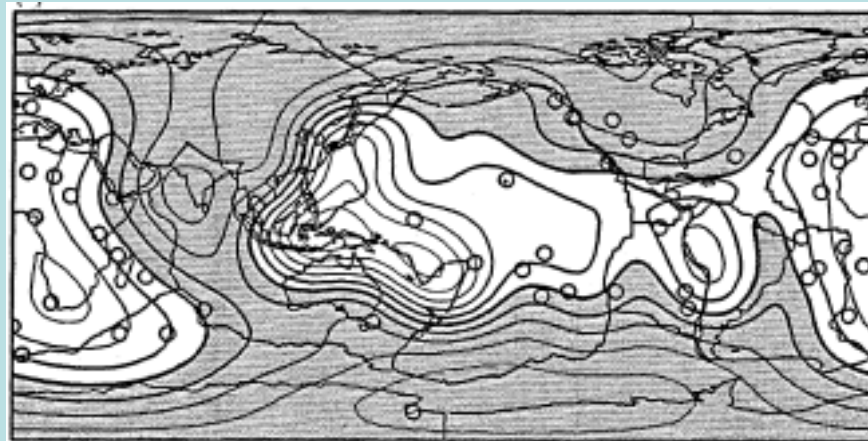


(Ritsema et al., 1999)

Explaining the geoid anomalies



Observed



Modeled using buoyancy derived from seismic models and subducted slabs.

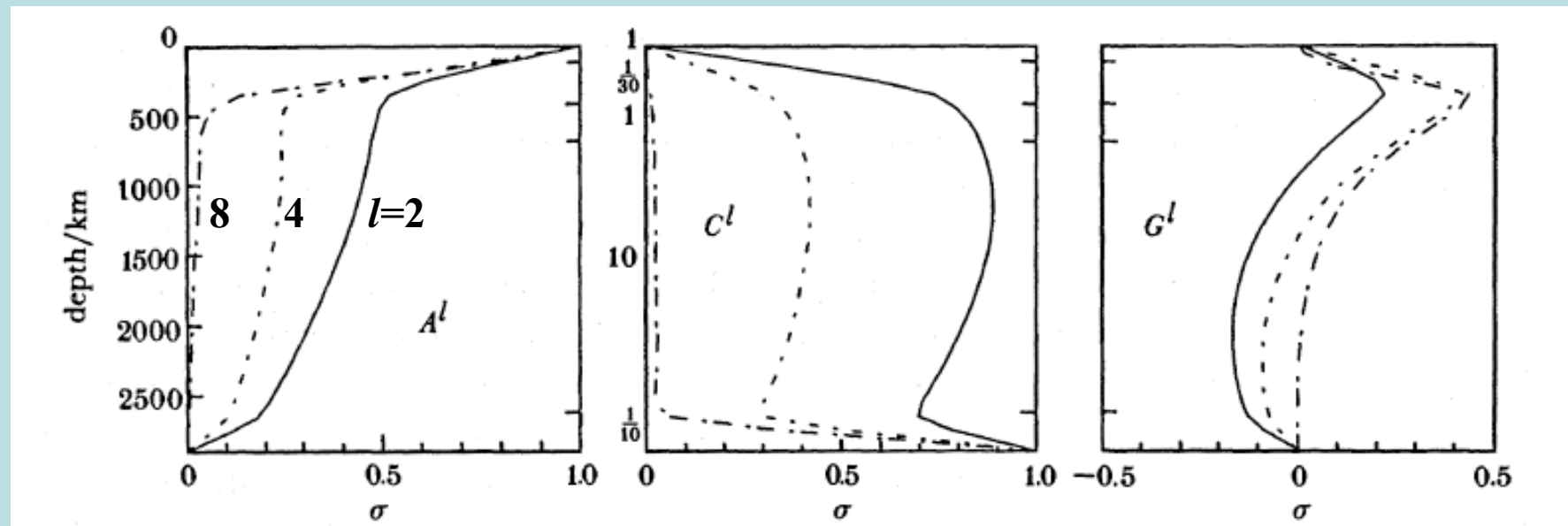
Hager and Richards, 1989

Long-wavelength geoid anomalies cannot be produced by crustal and lithospheric structure

Surface topo. kernel

CMB topo. kernel

Geoid kernel

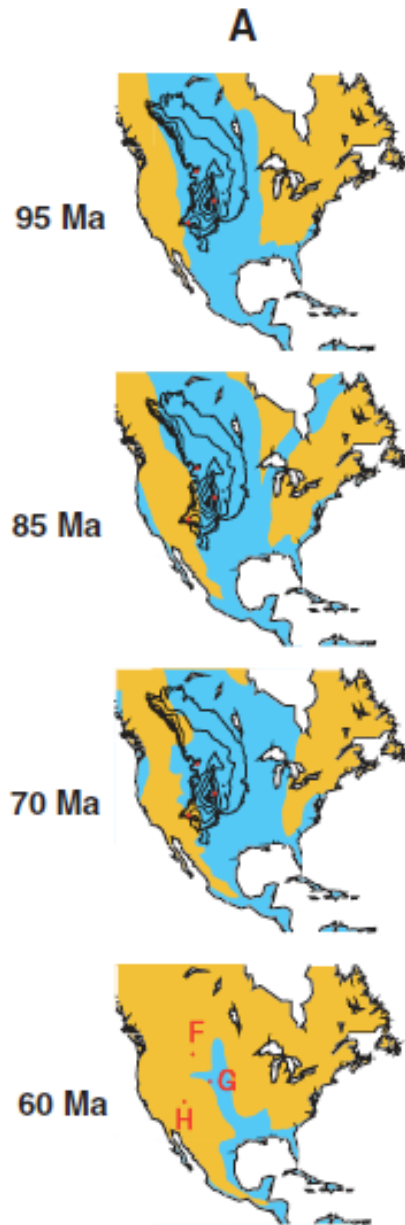


Hager & Richards, 1989

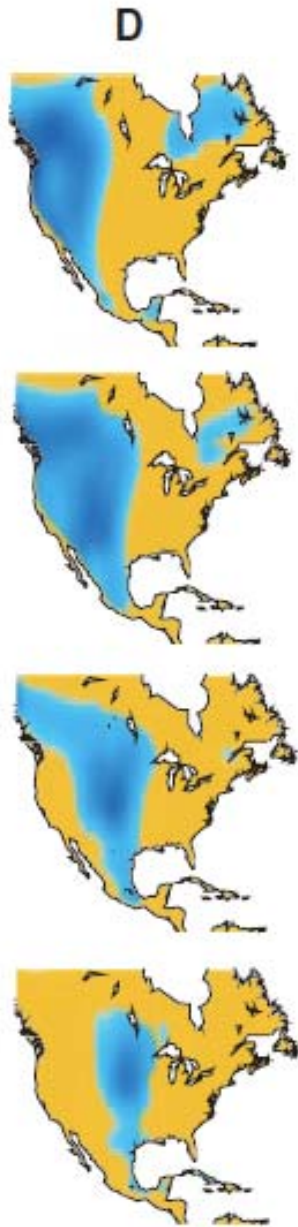
Mid-Cretaceous Seaways



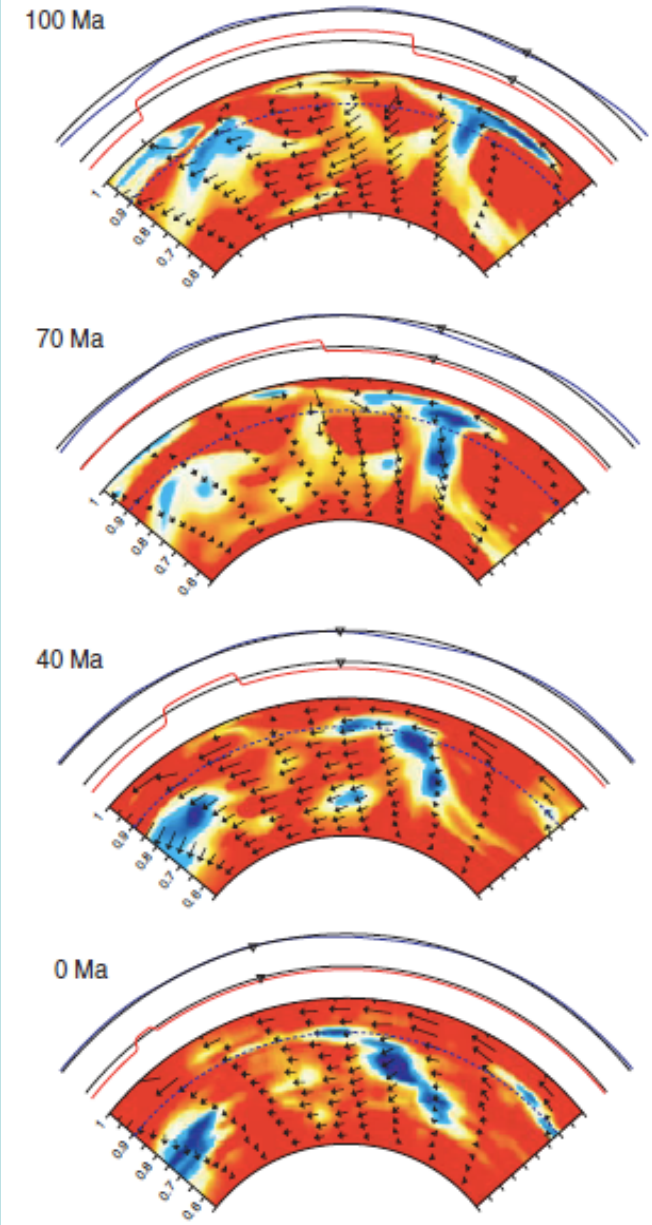
History of dynamic topography and vertical motion



Observed continental flooding



Modeled continental flooding



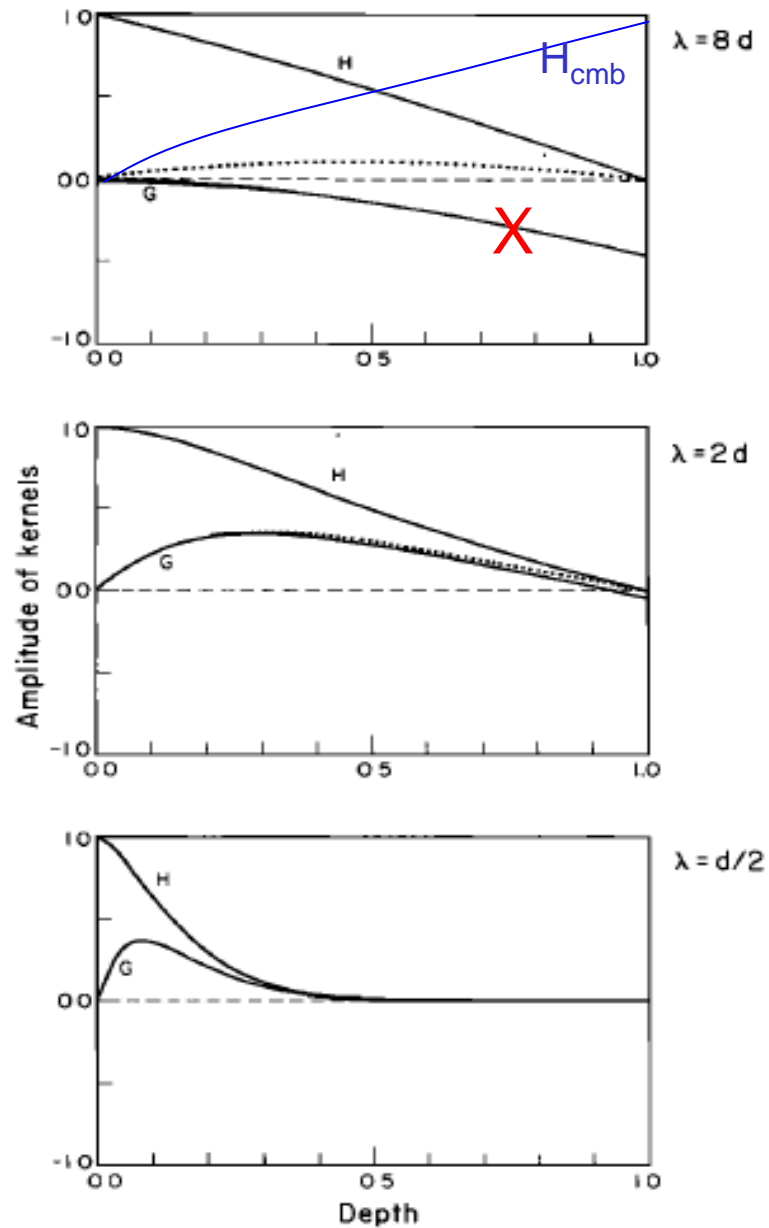
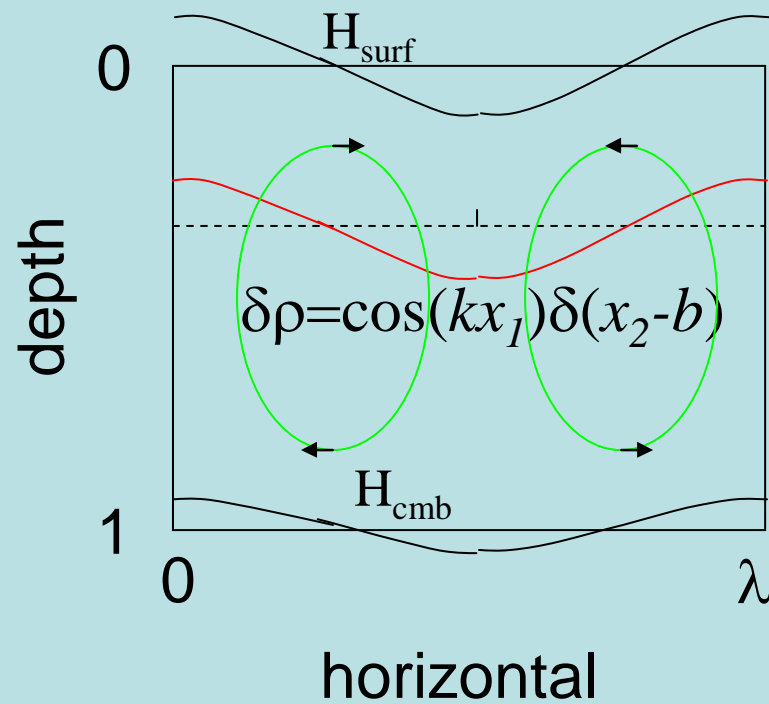
Liu et al., 2008; Mitrovica et al., 1989

More on dynamic topography and geoid

(Notes on topography and gravity
kernels follow Parsons and Daly [1983]
extensively.)

June 1, 2011

Topography and Geoid Kernels



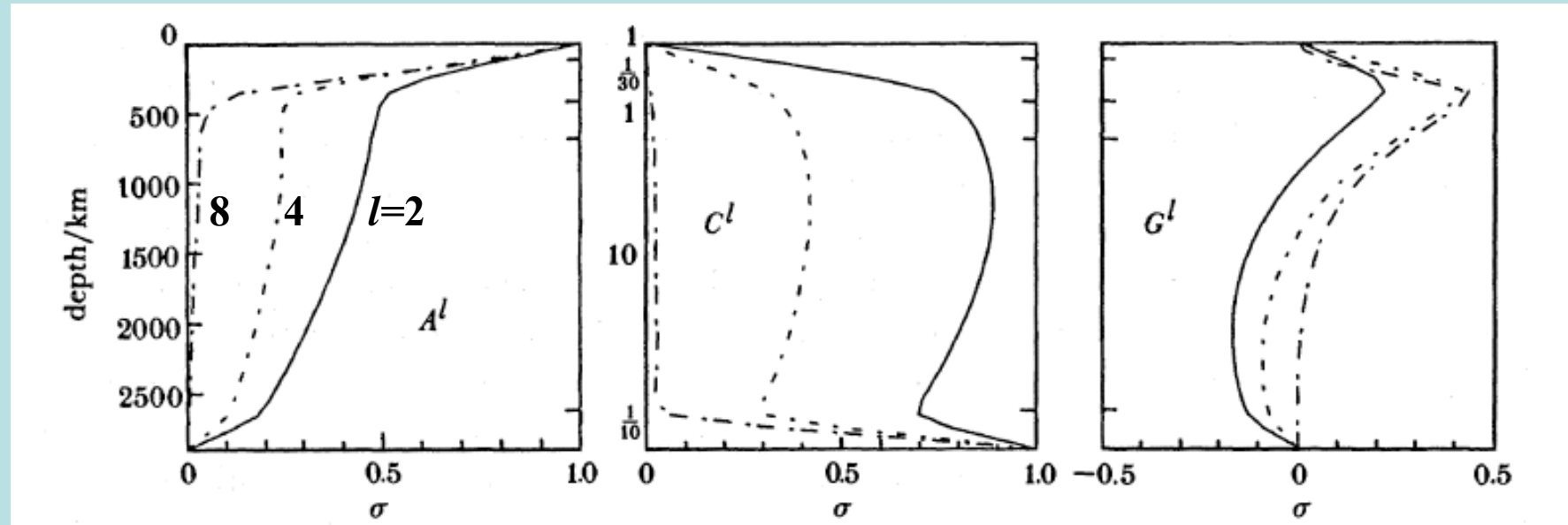
Parsons and Daly, 1983

Kernels in spherical geometries

Surface topo. kernel

CMB topo. kernel

Geoid kernel



$$\delta a^{lm} = \frac{1}{\Delta \rho_a} \int_c^a A^l(r) \delta \rho^{lm}(r) dr,$$

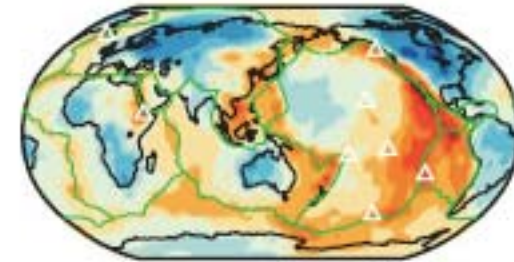
$$\delta c^{lm} = \frac{1}{\Delta \rho_{\text{CMB}}} \int_c^a C^l(r) \delta \rho^{lm}(r) dr,$$

$$\delta V_{(a)}^{lm} = \frac{4\pi\gamma a}{2l+1} \int_c^a G^l(r) \delta \rho^{lm}(r) dr,$$

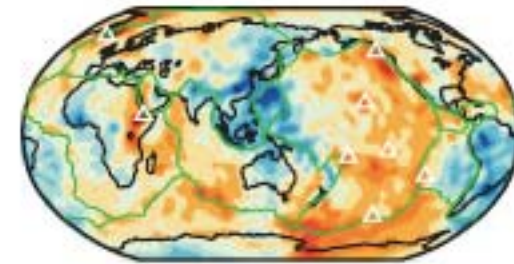
Hager & Richards, 1989

Mantle density
 $\delta\rho(\theta,\phi,r)$ can be
potentially
derived from
seismic models

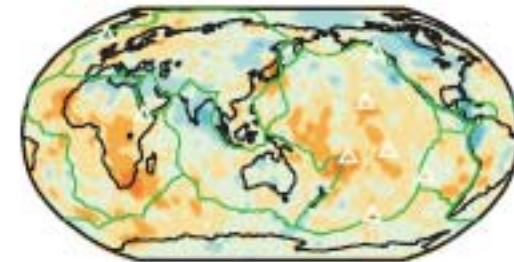
100 km
(7%)



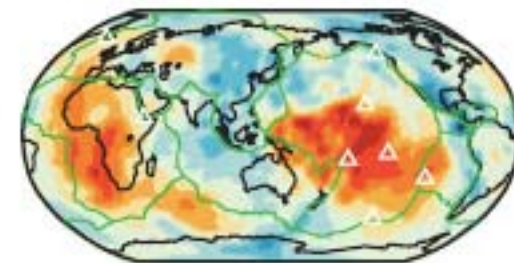
600 km
(2%)



1500 km
(2%)

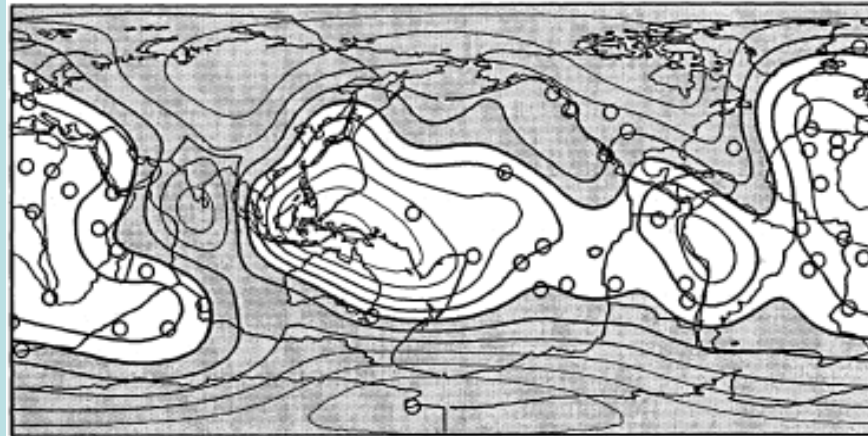


2800 km
(2%)

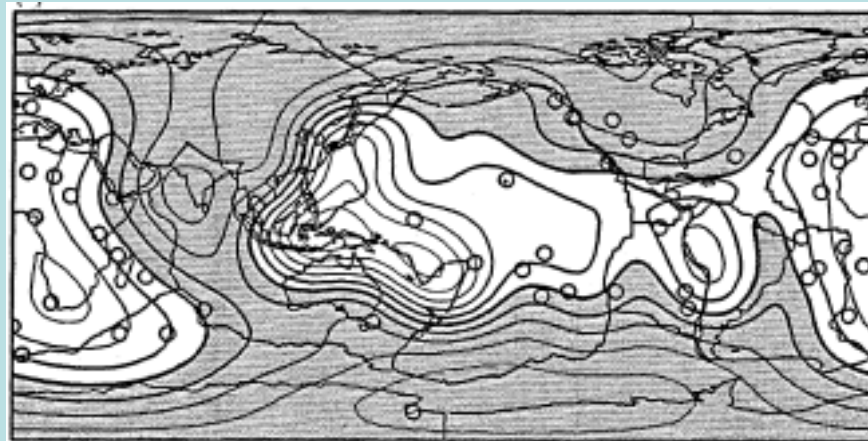


Ritsema et al., 2011

Explaining the geoid anomalies



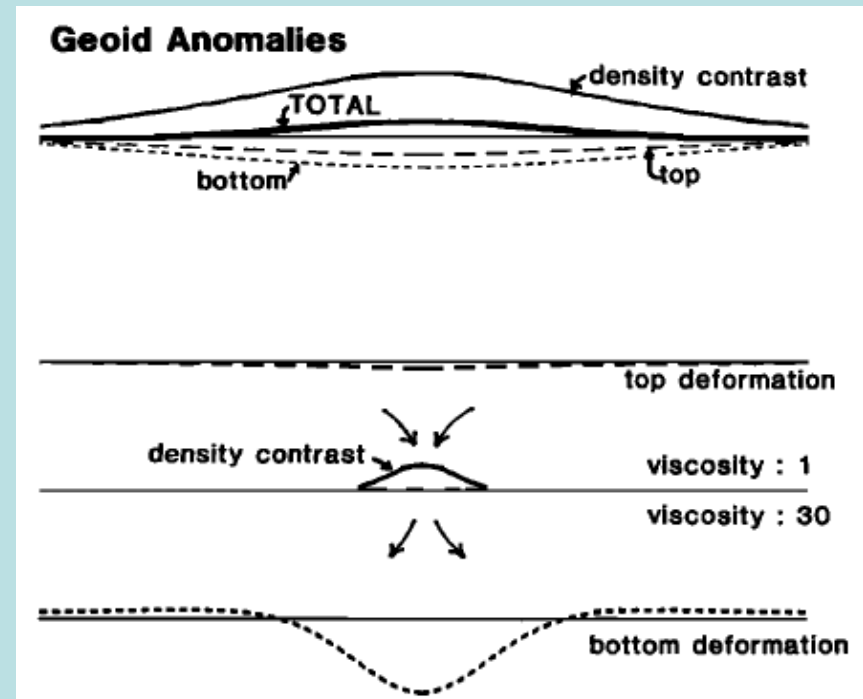
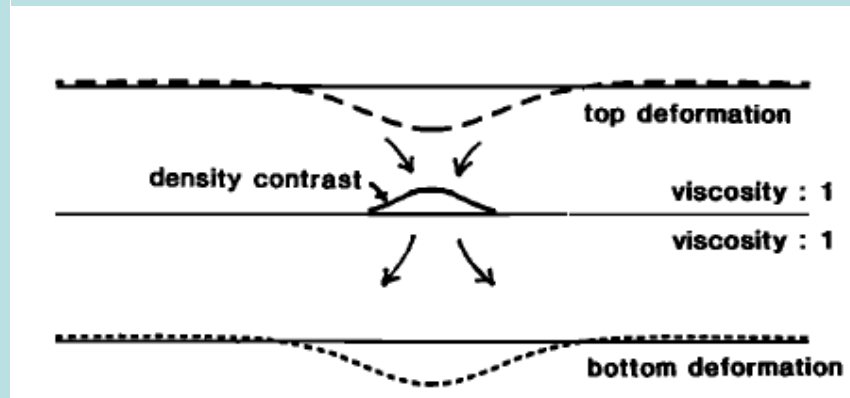
Observed



Modeled using buoyancy derived from seismic models and subducted slabs.

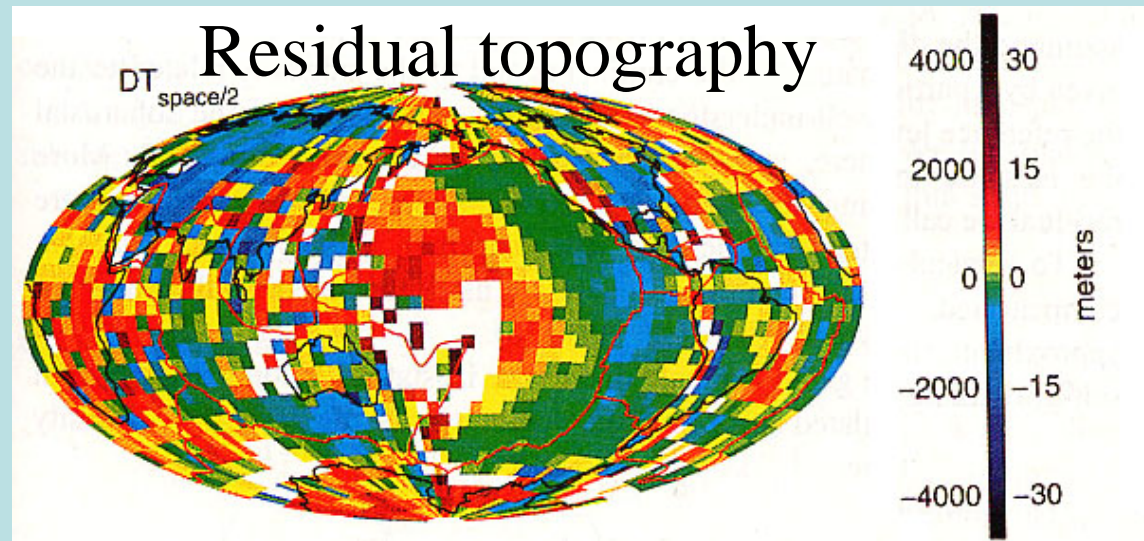
Hager and Richards, 1989

Vertical viscosity structure's effects on the surface geoid anomalies



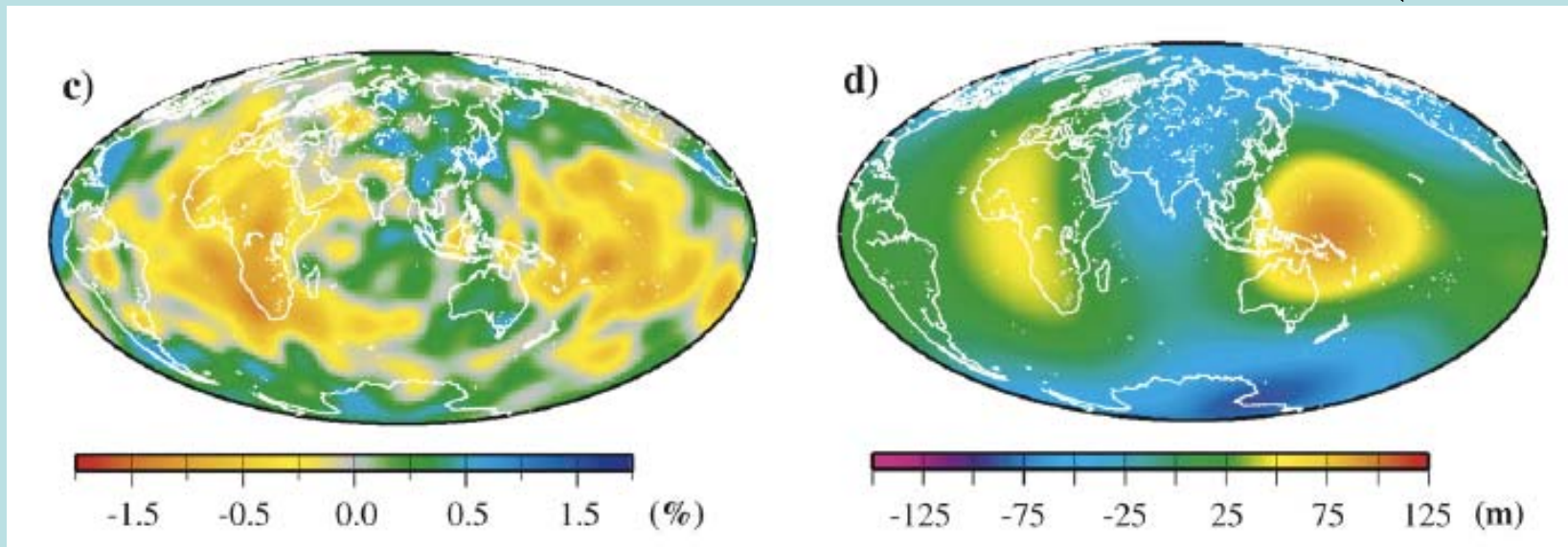
Hager, 1984

A case for dynamic topography



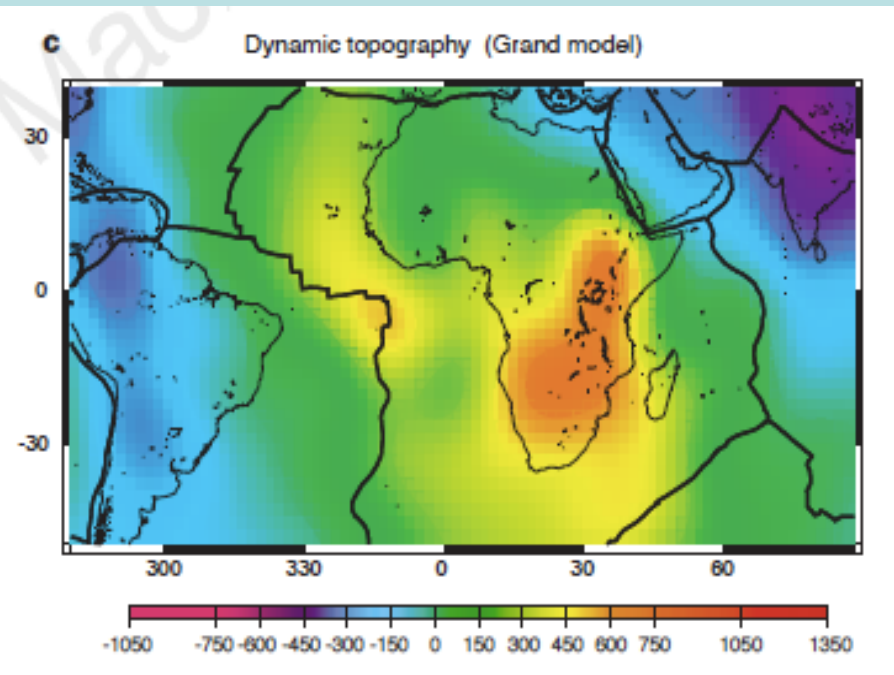
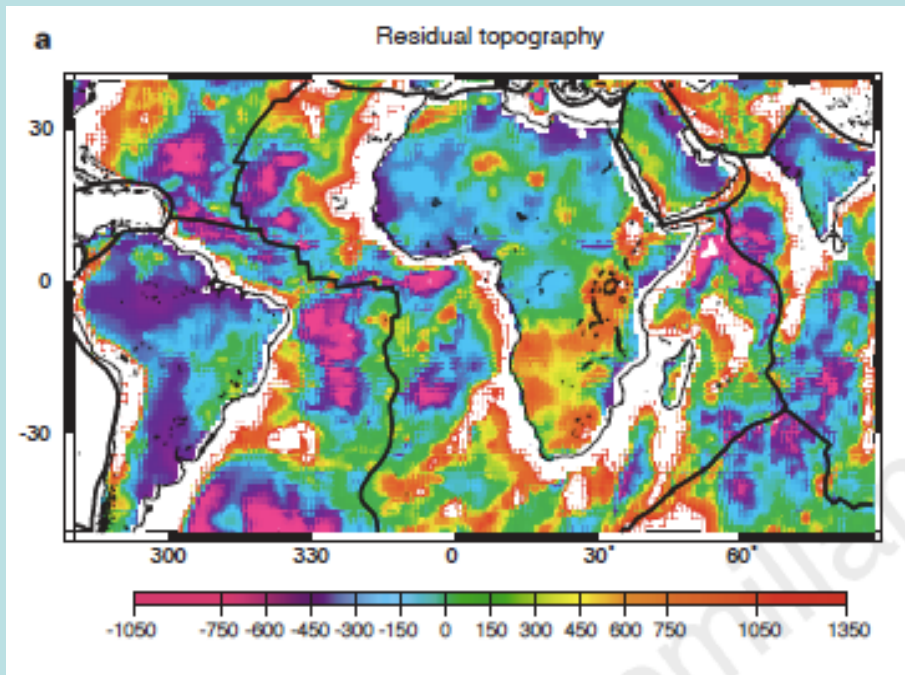
dV_s/V_s at 2300 km depth

Geoid anomalies (1=2 & 3)



(Ritsema et al., 1999)

African swell – residual topography relative to $\frac{1}{2}$ space cooling model



***Nybrade & Robinson, 1994;
Lithgow-Bertelloni & Silver, 1998***

Iceland, the Farallon slab, and dynamic topography of the North Atlantic

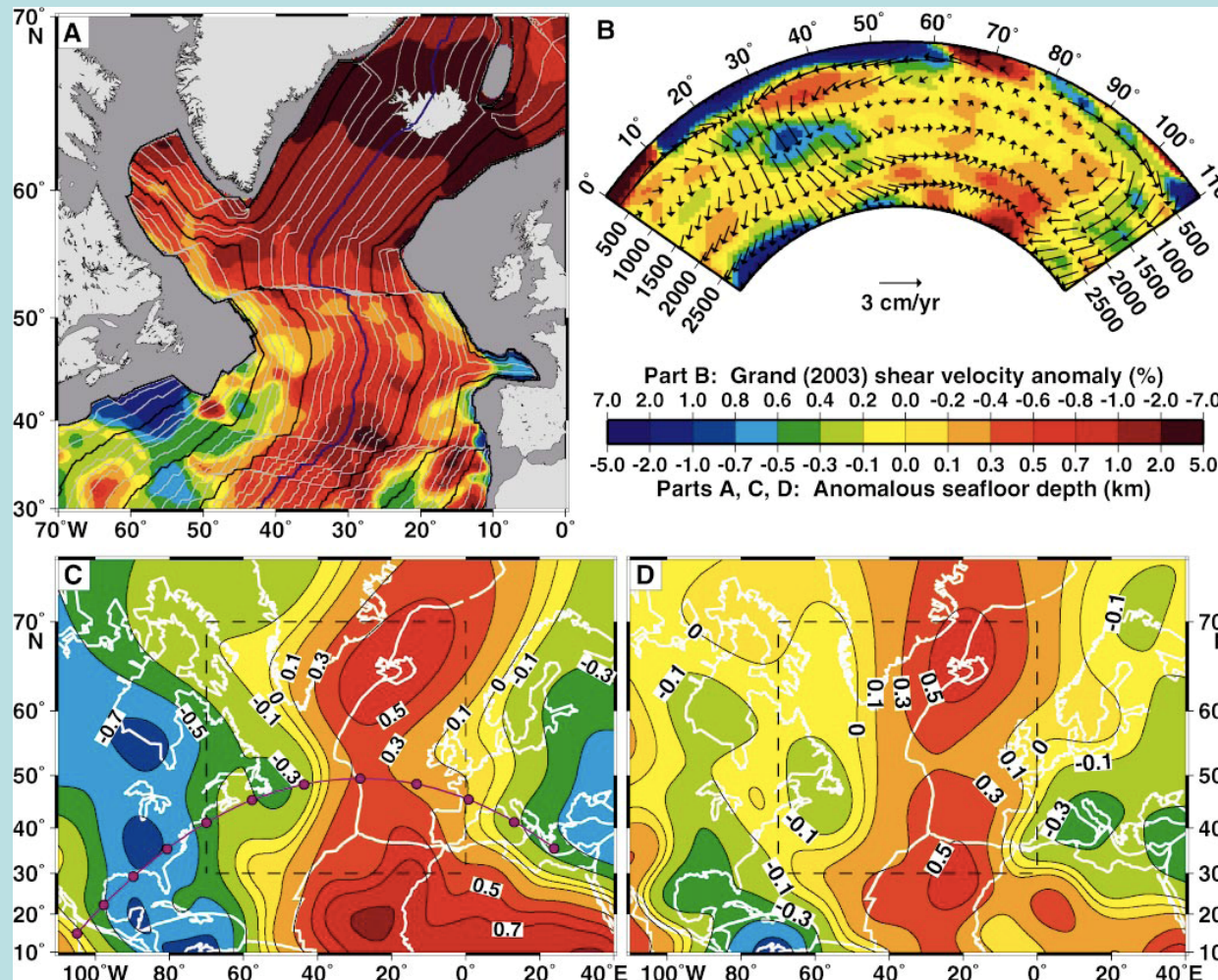
Clinton P. Conrad

Carolina Lithgow-Bertelloni

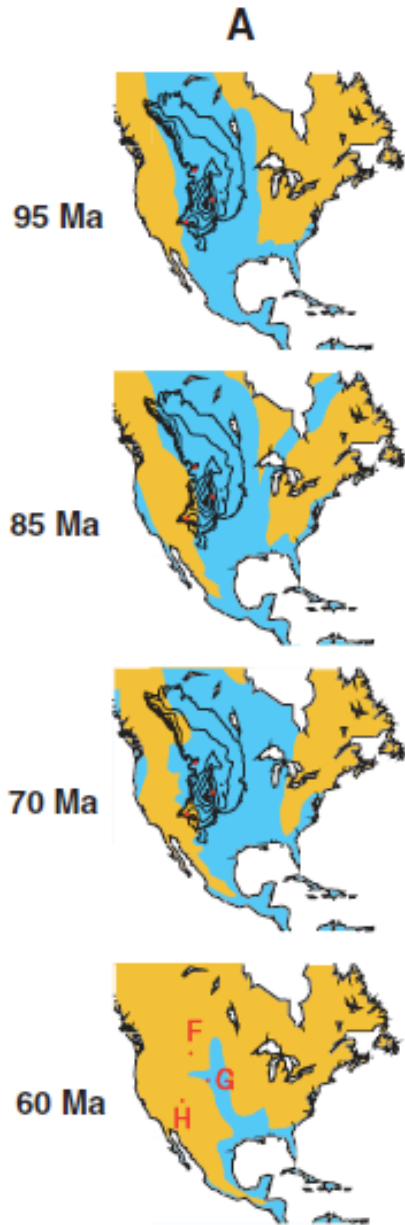
Keith E. Louden

} Department of Geological Sciences, University of Michigan, Ann Arbor, Michigan 48109, USA

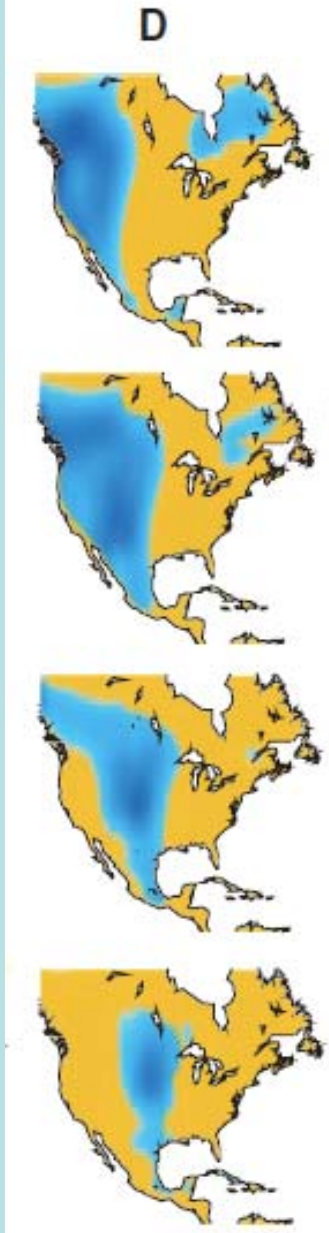
Department of Oceanography, Dalhousie University, Halifax, Nova Scotia B3H 4J1, Canada



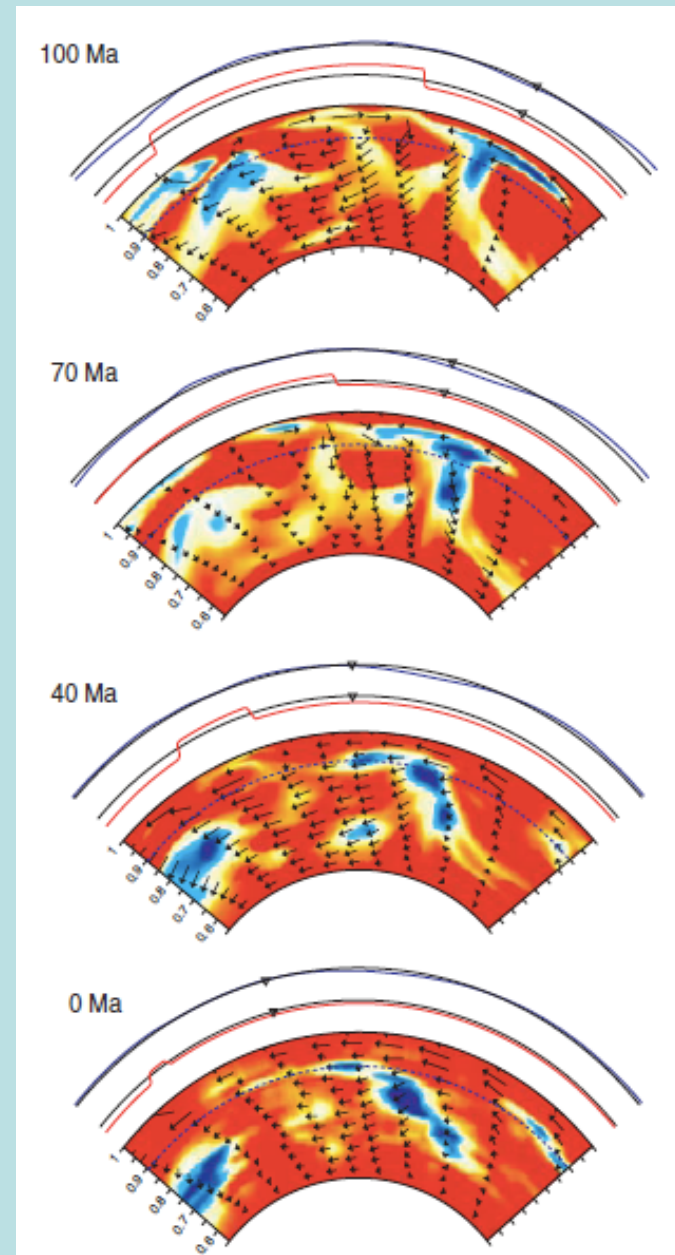
History of dynamic topography and vertical motion



Observed continental flooding



Modeled continental flooding



Liu et al., 2008; Mitrovica et al., 1989